Weather and Climate Extremes 23 (2019) 100194

Contents lists available at ScienceDirect

Weather and Climate Extremes

journal homepage: www.elsevier.com/locate/wace

Analysis of climate extreme indices over the Komadugu-Yobe basin, Lake Chad region: Past and future occurrences

O.E. Adeyeri[a,c,*], A.E. Lawin[b], P. Laux[c], K.A. Ishola[d], S.O. Ige[e]

[a] Graduate Research Programme on Climate Change and Water Resources, West African Science Service Centre on Climate Change and Adapted Land Use, University of Abomey-Calavi, Benin
[b] Laboratory of Applied Hydrology, National Water Institute, University of Abomey-Calavi, Benin
[c] Institute for Meteorology and Climate Research Atmospheric Environmental Research, Karlsruhe Institute of Technology, Germany
[d] Department of Geography, National University of Ireland, Maynooth, Ireland
[e] Nigerian Meteorological Agency, National Weather Forecasting and Climate Research Centre, Nigeria

ARTICLE INFO

Keywords:
Homogeneity
Climate extreme indices
Linear trends
Bias correction
Komadugu-Yobe basin
Lake Chad region

ABSTRACT

This study investigates trends of climate extreme indices in the Komadugu-Yobe Basin (KYB) based on observed data of the period 1971–2017 as well as regional climate model (RCM) simulations for the historical period (1979–2005), the near future (2020–2050), and the far future (2060–2090). In order to correct change points in the time historical series, the Adapted Caussinus Mestre Algorithm for homogenising Networks of Temperature series homogeneity test is used. The magnitude of the linear trends is estimated using the Sen's slope estimator and Mann-Kendall's test is performed to check the statistical significance of the trends. Future trends are assessed using the ensemble mean of eight regional climate model data under two emission scenarios, provided by the Coordinated Regional Climate Downscaling Experiment (CORDEX). Therefore, the projected rainfall and temperature have been corrected for biases by using empirical Quantile Mapping. In the observations, warm spell duration, warm day-, and warm night frequencies exhibit statistically significant positive trends. Although there is a positive trend in the annual total rainfall, the number of consecutive wet (dry) days decreases (increases). The future climate also shows a continuing positive trend in the temperature extreme indices as well as more frequent extreme rainfall events. Therefore, it is pertinent for decision-makers to develop suitable adaptation and mitigating measures to combat climate change in the Basin.

1. Introduction

In recent decades, there has been an increase in the frequency, intensity and extent of the impact of natural disasters on the environment which is a concern to many nations. This has been attributed to climate change and environmental degradation (Lyon and DeWitt, 2012). Ly et al. (2013) argued that climate variability is mainly associated with increasing concentration of anthropogenic greenhouse gases in the atmosphere. This has resulted in global warming.

Over the Sudanian, Sahelian and Sahelo-Saharan ecological zones of West Africa, there has been an increasing trend of both maximum and minimum temperatures with minimum temperatures increasing more rapidly (Ly et al., 2013). Abatan et al. (2017a) examined the trend in absolute indices of temperature extremes over Nigeria linking it with the Northern Atlantic Oscillation (NAO) for the period 1971–2012. They found out that warming is most pronounced in the southern part of the country with a significant increasing trend. Abatan et al. (2017b) investigated the trends in mean and extreme temperatures over Ibadan, Southwest Nigeria, between 1971 and 2012 using ERA-20C reanalysis data (Poli et al., 2016) and reported increasing annual and seasonal mean minimum temperatures with a non-significant decrease in the annual mean maximum temperature. The coldest night also shows greater warming trend than on the coldest day.

In many West African countries, the frequency of flood events has increased which had led to the loss of human lives and properties (Attogouinon et al., 2017). This has been attributed to climate change (Adeyeri et al., 2017a). Abiodun et al. (2017) examined the impacts of climate change on characteristics of extreme precipitation events over four African coastal cities under two future emission scenarios (RCP4.5 and RCP8.5). They reported an increase in dry spells and a decrease in wet days over the four cities in the future (2031–2065). Results from other studies (e.g. Shongwe et al., 2010; Mason and Joubert, 1997)

* Corresponding author. Graduate Research Programme on Climate Change and Water Resources, West African Science Service Centre on Climate Change and Adapted Land Use, University of Abomey-Calavi, Benin.
E-mail address: cyndyfem@gmail.com (O.E. Adeyeri).

https://doi.org/10.1016/j.wace.2019.100194
Received 20 May 2018; Received in revised form 22 November 2018; Accepted 8 January 2019
Available online 14 January 2019

showed that the modifications in extreme weather and climate events in Africa can be attributed to climate change. For example, Mason and Joubert (1997) projected an increasing intensity of extreme rainfall over South Africa using an ensemble of global circulation models (GCMs). Shongwe et al. (2010) also projected an increasing intensity of dry extremes over South-western Africa in summer months for the years of 2046–2065 and 2081–2100, respectively. As a result of the coarse spatial resolution of the GCM simulations and projections used in the studies, it is difficult to account for the impact of the complex topography on synoptic-scale features and mesoscale atmospheric systems that favour extreme precipitation. To bridge this gap between large scale and local scale, a number of studies have downscaled GCM projections with RCMs (e.g. Engelbrecht et al., 2009; Klutse et al., 2014; Dieng et al., 2017).

Although many studies have utilised an RCM to investigate the changes in the long-term means of temperature and rainfall over Africa, just a few have examined the influence of climate change on climate extremes. It is also worthy to note that many studies have explored the suitability of single RCMs in downscaling GCM simulations (e.g. Dosio and Panitz, 2016).

The Coordinated Regional Climate Downscaling Experiment (CORDEX, Nikulin et al., 2012) initiated international efforts in regional climate downscaling and made the data accessible publicly. Regardless of this development, only a few studies have utilised the CORDEX dataset in providing multi-RCM future projections for climate extremes in Africa e.g. on precipitation extremes over Southern Africa (Pinto et al., 2016). It is worthy to note that studies from other parts of the world (e.g. Zhang et al., 2006; Im et al., 2011; Xu and Xu, 2012; Pinto et al., 2016) have evaluated the trend in future projections of climate extremes using RCMs. However, biases in temperature and precipitation simulations as a result of discretization and spatial averaging within grid cells hinder the direct use of climate simulations for impact studies (e.g. Teutschbein and Seibert, 2013). Hence, it is important to bias-correct model output before using it for impact studies. Furthermore, the use of extreme indices for climate extremes analysis is based on the exceeding threshold or probability of occurrence of a given variable. Results from various studies in Africa (e.g. Ly et al., 2013; Abatan et al., 2017a) showed no uniform pattern in the trend of annual precipitation as it depends on the locality. A faster increase in minimum temperature over maximum temperature is seen as a contributing factor to a smaller diurnal temperature range (Ly et al., 2013). Overall, the different patterns of the above results encourage continuing analysing the climate extremes for several spatial scales (e.g. the regional-, local-, or watershed scale).

From current understanding, the environmental impacts associated with increasing extreme climate events and constrained by anthropogenic climate change will attract severe costs especially to vulnerable economies (like of the study area) in West Africa.

Therefore, the present paper aims at assessing the trends in extreme rainfall and temperature indices in the Komadugu-Yobe Basin (KYB) of the Lake Chad Basin by using station observations (1971–2017), regional climate model simulations for the past (1979–2005), the near future (2020–2050) and the far future (2060–2090) as well as validation period from station observations (1979–2005). To this regard, six temperature indices (Table 1), namely cool day frequency (tx10p), warm day frequency (tx90p), cool night frequency (tn10p), warm night frequency (tn90p), warm spell duration indicator (wsdi), diurnal temperature range (dtr), as well as six precipitation indices, namely maximum 5-days rainfall (rx5day), consecutive dry days (cdd), consecutive wet days (cwd), very wet days (r95p), extremely wet days (r99p), and annual total rainfall (prcptot) have been analysed for these periods. This study will provide information as regards the overall understanding of past and future climate extreme events in the basin which could trigger relevant adaptation as well as mitigation strategies suitable for the basin.

2. Study area

The study area is the KYB which falls predominantly within the Sudan and Sahel savannah ecological zone in South-Western Niger and North-Eastern Nigeria with a total area of 150,000 km^2 with 95% of the basin's water in Nigeria (Odunuga et al., 2011). The vegetation is naturally dominated by shrubs and dense grasslands with scattered trees. The basin is drained by the Komadugu Yobe and the Komadugu Gana river sub-systems, which both flow as the Yobe River into the Lake Chad. KYB is a sub-basin which represents 35% of the larger Lake Chad Basin (Fig. 1). The river systems network and wetlands in the KYB supports different economic activities and ecological processes which include forest regeneration, pastoralism, fish production, trading and recession agriculture. Presently, over 20 million people depend on these activities in the basin. The wetlands of the KYB play host to different ecosystems.

At the core of the Sahel expanse, the KYB is characterised by a semi-arid climate, severe drought and high rainfall variability (Thompson and Polet, 2000). Severe drought is a frequent hazard which leaves communities vulnerable and a reduced adaptive capacity to climate change. Due to the joint effects of the construction of two large dams in the 1970s, water abstraction as a result of large-scale irrigation and regional climate change, KYB water flow has reduced by 35% (IUCN, 2006). To this effect, the Komadugu Gana River no longer reaches the Yobe River, which has drastically reduced its contribution to Lake Chad flow from 10% to 1% in a space of two decades, hence, the shrinking of Lake Chad over the last 40 years (IUCN, 2006). The rain season is between May and October. The mean annual rainfall from 1979 to 2015 ranges between 240 mm in the northern sector and 1060 mm in the southern sector (Adeyeri et al., 2017b) while the maximum temperature range is between 27.4 °C in the southern part and 35 °C in the north part. Annual potential evaporation varies between 1800 mm and 2400 mm over the basin (IUCN, 2006). The relative humidity is 40% per annum while the rate of evaporation is 203 mm per annum (Adeyeri et al., 2016). The KYB is seen to be of strategic, national and international value because of its important wetlands which are the origin of some internationally shared waters which are of immense significance to the local, national and international economy as well as the diplomatic relationships among different countries in the Lake Chad Basin (IUCN, 2006). It also has a great potential for ecology conservation.

3. Data and methods

Stations' daily rainfall, air minimum and maximum temperature archived by the Direction de la Meteorologie Nationale (DMN) of the Niger Republic and Nigeria Meteorological Agency (NiMet) were used for the analysis (Table 2). The climate data were quality controlled using the Rclimdex package (Zhang and Yang, 2004). In quality control, days with maximum temperature lesser than minimum temperature, outliers and negative precipitation values were checked. There was 100 percent data completeness after quality control. The quality controlled data series was checked and corrected for inhomogeneities using a multi-break method based Adapted Caussinus-Mestre Algorithm for homogenising Networks of Temperature series (ACMANT). A detailed

Table 1
Definitions of indices used in this study.

Indices	Name	Definition	Unit
Precipitation Indices			
rx5day	Maximum 5-days rainfall	Maximum 5-days rainfall	mm
cdd	Consecutive dry days	Maximum number of consecutive days with RR < 1 mm	days
cwd	Consecutive wet days	Maximum number of consecutive days with RR ≥ 1 mm	days
r95p	Very wet days	Annual total rainfall when RR > 95 percentile	mm
r99p	Extremely wet days	Annual total rainfall when RR > 99 percentile	mm
prcptot	Annual Total Rainfall	Annual total rainfall in wet day (RR > 1 mm)	mm
Temperature Indices			
dtr	Diurnal temperature range	Annual mean difference between tx and tn	°C
tx10p	Cool day frequency	Percentage of days with tx < 10th percentile	%
tx90p	Warm day frequency	Percentage of days with tx > 90th percentile	%
tn10p	Cool night frequency	Percentage of days with tn < 10th percentile	%
tn90p	Warm night frequency	Percentage of days with tn > 90th percentile	%
wsdi	Warm spells duration indicator	Annual count of days with at least 6 consecutive days with tx > 90th percentile	days

tn and tx are the daily minimum and maximum temperatures respectively, RR is daily precipitation amount.

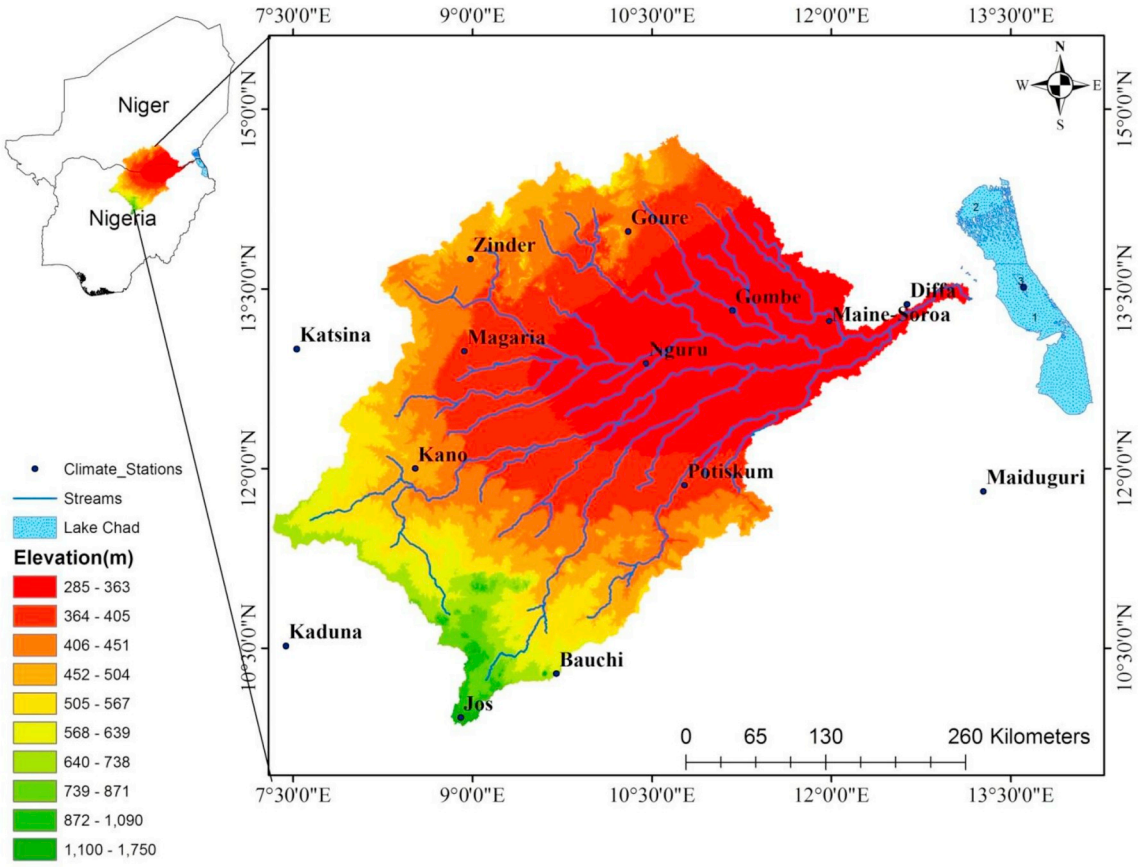

Fig. 1. Map of Komadugu-Yobe basin.

scientific description on ACMANT can be found in Domonkos, (2014, 2015) and Domonkos and Coll (2017). ACMANT has been successfully used in homogenising climate variables (precipitation, temperature and relative humidity) with good performances (Domonkos, 2015, Domonkos and Efthymiadi, 2013; Pérez-Zanón et al., 2015; Domonkos and Coll, 2018; Barbara et al., 2018). However, the performance of homogenisation improves with more network stations (Domonkos and Coll, 2017; Gubler et al., 2017). An ensemble of CORDEX data comprising of eight GCMs (Table A.1.) dynamically downscaled by one RCM, i.e. the RCA4 (Swedish Meteorological and Hydrological

Table 2
List of stations in the basin used for the study.

s/n	Country	Station	Lat	Long	Data Range
1	Niger	Diffa	13.31	12.61	1979–2017
2	Niger	Goure	13.98	10.3	1979–2017
3	Niger	Zinder	13.75	8.98	1971–2017
4	Niger	Magaria	12.98	8.93	1979–2017
5	Niger	Maine-Soroa	13.23	11.98	1971–2017
6	Nigeria	Maiduguri	11.81	13.27	1971–2017
7	Nigeria	Potiskum	11.86	10.77	1979–2017
8	Nigeria	Katsina	13	7.53	1971–2017
9	Nigeria	Kaduna	10.52	7.44	1971–2017
10	Nigeria	Kano	12	8.52	1971–2017
11	Nigeria	Gombe	13.32	11.17	1972–2017
12	Nigeria	Nguru	12.88	10.45	1971–2017
13	Nigeria	Bauchi	10.28	9.7	1971–2017
14	Nigeria	Jos	9.92	8.9	1971–2017

Institute-Rossby Centre Atmosphere model version 4) which has a resolution of 0.44° × 0.44° was used for the projection between near future (2020–2050) and far future (2060–2090) under two representative concentration pathway (RCP 4.5 and RCP 8.5) while the simulated historical was between 1979 and 2005. RCA4 convection scheme is based on the Bechtold Kain-Fritsch. Further description of the physical parameterizations, domain set up and lateral boundary conditions can be found in Samuelsson et al. (2011). The RCP is the pathway of the cumulative greenhouse gases emission by humans from all sources in part per million volumes (ppmv). RCP 45 is the medium stabilization scenario when carbon dioxide emission is at 650ppmv while RCP 85 is the very high baseline emission scenario when carbon dioxide emission is at 1370ppmv. This RCM is chosen due to its performance over West Africa and particularly its ability to adequately reproduce West Africa rainfall regimes (Akinsanola et al., 2017; Yira et al., 2017; Alamou et al., 2017). The station point data for both historical CORDEX (1979–2005) and projection phase (2020–2050, 2060–2090) were extracted from the CORDEX data. The climate extreme indices of the homogenised validation period (1979–2005), CORDEX simulated historical period (1979–2005), near future (2020–2050) and far future (2060–2090), as well as the homogenised data series for the observed historical period were calculated using the Rclimdex package (Zhang and Yang, 2004).

3.1. Detecting breakpoints, step function fitting and homogenisation of climate data series

Quality climate data series especially long-term are necessary for observing and studying climate variability and change. To obtain a high quality and reliable climate data series free of errors and inhomogeneities, the climate data series must be homogenised (Peterson et al., 1998; Aguilar et al., 2003; Trewin, 2010; Acquaotta and Fratianni, 2014). Inhomogeneity in climate data can be caused by instrument repositioning, changes in reading instruments' time, station relocations etc. (Acquaotta et al., 2016). The most frequent form of climate data series inhomogeneity is the change or break point which occurs as a result of the sudden shift of the means (Domonkos and Coll, 2017). Hierarchic structures (e.g. Alexandersson and Moberg, 1997) can be used to individually correct a set of breaks or can be done jointly using suitable mathematical tools. Joint treatments have advantages over hierarchic methods if the time series has multiple breaks (Lindau and Venema, 2016). Efficiency assessments demonstrate that multiple break techniques (joint detection of inhomogeneities or bivariate detection) generally outdo other homogenisation approaches (Domonkos et al., 2011; Venema et al., 2012).

In ACMANT, breakpoints are detected using both univariate and bivariate detection methods. The task of best step function fitting as a model of data series is the same as the minimizing the variance of internal distances and maximizing the variance of external distances (Lindau and Venema, 2013). The correction for inhomogeneity is presented as follows (Domonkos and Coll, 2017);

$$\boldsymbol{u_{s,j}} = \left\{ x = \begin{array}{c} \boldsymbol{min\ \ if\ \ sign}(\boldsymbol{t_{s,j,x}}) = \boldsymbol{c\ for\ every\ x} \\ \{1, \boldsymbol{N'_{s,j}}\}^{|\boldsymbol{t_{s,j,x}}|} \\ 0\ \boldsymbol{if\ \ sign}(\boldsymbol{t_{s,j,x}}) \neq \boldsymbol{c\ for\ any\ x} \in \{1, \boldsymbol{N'_{s,j}}\} \\ c = 1\ or\ c = -1 \end{array} \right\} \quad (1)$$

where; u is the adjustment term, s is the reference series serial number, $\boldsymbol{x}$ is an ensemble homogenisation serial number, N′ is the total number of usable reference series at a particular iteration step, c is a parameter, j is the year.

3.2. Analysis of climate extreme trends

In analysing the climate extreme trend, the Mann-Kendall statistic was performed on the homogenous climatic time series while the magnitude of the trend was calculated using the Sen's slope estimator (Vincent et al., 2005).

The Mann-Kendall statistic tests whether to accept the alternative hypothesis (H_a) which states the presence of a monotonic trend or to reject (H_o), the null hypothesis which states that no monotonic trend occurred.

The Mann-Kendall statistic is given as:

$$\boldsymbol{S} = \sum_{k=1}^{n-1} \sum_{j=k+1}^{n} \boldsymbol{Sgn}(\boldsymbol{x_j} - \boldsymbol{x_k}) \quad (2)$$

Where x_j and x_k are sequential data values for the time series data of length n. The Sgn series is defined as

$$\boldsymbol{Sgn}(\boldsymbol{x_j} - \boldsymbol{x_k}) = \begin{cases} 1\ if\ \boldsymbol{x_j} > \boldsymbol{x_k} \\ 0\ if\ \boldsymbol{x_j} = \boldsymbol{x_k} \\ -1\ if\ \boldsymbol{x_j} < \boldsymbol{x_k} \end{cases} \quad (3)$$

The statistic S, the mean E(S) and the variance V(S) can be computed as;

$$\boldsymbol{E}(\boldsymbol{S}) = 0 \quad (4)$$

$$\boldsymbol{V}(\boldsymbol{S}) = \frac{1}{18}\left\{\boldsymbol{n}(\boldsymbol{n}-1)(2\boldsymbol{n}+5) - \sum_{i=1}^{n} \boldsymbol{t_i}[(\boldsymbol{t_i}-1)(2\boldsymbol{t_i}+5)]\right\} \quad (5)$$

where t_i is the extent of any given tie. Σt_i denotes the summation over all ties and is only used if the data series contain tied values. The standard normal variate Z is calculated by:

$$\boldsymbol{Z} = \begin{cases} \frac{\boldsymbol{S}-1}{\sqrt{\boldsymbol{V}(\boldsymbol{S})}}\ if\ S > 0 \\ 0\ if\ S = 0 \\ \frac{\boldsymbol{S}+1}{\sqrt{\boldsymbol{V}(\boldsymbol{S})}}\ if\ S < 0 \end{cases} \quad (6)$$

The Sen's slope estimator is calculated as;

$$Q_j = \frac{(x_k - x_l)}{(k - l)} \text{ for } j = 1, \ldots R \quad k > l \tag{7}$$

where xk and xl are values at times k and l respectively. Qj is a Sen's estimator of slope which is the median of these R values. If there are n values of xk present in each time period, then

$$R = n(n - 2)/2 \tag{8}$$

where n is the number of time periods. The R values of Q_j are ranked by $Q_1 \leq Q_2 \leq \cdots \leq Q_{R-1} \leq Q_R$ and

$$Sen's estimator = \begin{cases} Q_{(R+1)/2} \text{ if } R \text{ is odd} \\ 0.5 * \left(Q_{R/2} + Q_{(R+2)/2} \right) \text{if } R \text{ is even} \end{cases} \tag{9}$$

3.3. Bias correction of rainfall and temperature time series

The empirical Quantile Mapping (QM) bias correction method (Teutschbein and Seibert, 2013), which is recognized to efficiently correct rainfall and temperature output of RCMs, has been used to correct the daily time series data in order to project the future changes in climate extremes under two Representative Concentration Pathways (RCP 4.5 and RCP 8.5) in the basin.

The correction aims to adjust the distribution of daily CORDEX time series data with the distribution of daily stations' observed time series using a transfer function (k).

The transformation can be formulated as below (Gudmundsson et al., 2012):

$$Observed = k(CORDEX) \tag{10}$$

If the series has a known distribution, the transformation is defined as:

$$Observed = F_O^{-1}(F_s(CORDEX)) \tag{11}$$

where F_s is the Cumulative Distribution Function (CDF) of CORDEX and F_O^{-1} is the inverse CDF of Observed.

The bias-corrected CORDEX data is divided into two parts; the historical phase (1979–2005) as well as the projection phase - the near future (2020–2050) and far future (2060–2090) under the RCP 4.5 and the RCP 8.5.

3.4. Validation of RCM

To test the ability of the RCM output to reproduce the climate extreme characteristics, both the raw CORDEX output and the bias-corrected CORDEX output have been used to analyse the temperature and precipitation indices over the basin between 1979 and 2005. The results have been compared with the temperature and precipitation indices output from the homogenised observed data for the validation period (1979–2005). The performance evaluation criteria that are used include the root mean square error, percentage bias, mean square error and standard deviation. Furthermore, results of the indices trends for both bias-corrected CORDEX and observed data for the validation period outputs have been analysed and compared spatially to verify the robustness of the bias-corrected CORDEX in reproducing the extreme indices.

3.5. Interpolation

The Inverse Distance Weighting (IDW) interpolation technique has been used to spatially interpolate the climate extreme patterns between the observation stations. The IDW averages the weights of observation values after which the interpolated points' neighbours have been identified (Shepard, 1968):

$$w(d) = \frac{1}{d^p}, \; p > 0 \tag{12}$$

where p is the number of points, d is the distance between points, w is the weighting function.

4. Results

4.1. Temperature indices

In Table 3, an overall positive trend is observed in warm day frequency, warm night frequency and warm spell duration while the cold night frequency has an overall negative trend over the entire stations for the observed historical period (1971–2017). The cool day frequency in most stations shows statistically significant negative slope with two stations having statistically significant positive slopes. The cool night frequency has statistically significant negative trends for all stations except Kano and Jos with a not-significant negative trend. Warm day

Table 3
Mann–Kendall (Modified MK) test (at 5% significant level) for observed historical period (1971–2017). Bold values represent significant change in trend. For more information about the location of the stations, please see Fig. 1.

Stations	Temperature Indices						Rainfall Indices					
	tx10p	tx90p	tn10p	tn90p	wsdi	dtr	rx5day	cdd	cwd	r95p	r99p	prcptot
Bauchi	**−0.102**	**0.332**	**−0.310**	**0.389**	**0.446**	**−0.021**	**1.489**	0.176	−0.030	**8.283**	**5.223**	**9.908**
Diffa	**−0.318**	**0.916**	**−0.145**	**0.409**	**2.383**	**0.087**	0.028	**1.415**	**0.047**	−0.989	−0.607	**4.054**
Gombe	**−0.054**	**0.144**	**−0.433**	**0.599**	**0.286**	**−0.084**	**1.159**	0.336	−0.055	**4.006**	**2.215**	2.188
Goure	0.179	**0.595**	**−0.303**	**0.207**	**1.417**	−0.005	**0.846**	0.054	−0.025	**3.806**	0.814	**5.365**
Jos	**−0.116**	**0.646**	−0.043	**0.845**	**1.949**	0.008	**−0.634**	−0.036	−0.023	−1.847	−0.994	−0.394
Kaduna	−0.05	**0.36**	**−0.23**	**0.426**	**0.498**	**−0.009**	−0.047	0.629	−0.008	−0.352	0.046	−0.616
Kano	**−0.101**	**0.514**	−0.025	**0.39**	**1.237**	0.014	**2.952**	0.259	0.000	**9.656**	**3.833**	**19.394**
Katsina	**−0.117**	**0.542**	**−0.066**	**0.549**	**1.228**	0.003	−0.342	0.097	0.014	1.582	0.256	4.010
Magaria	0.127	**0.344**	**−0.491**	**0.644**	**0.631**	**−0.077**	−1.019	**1.23**	−0.025	−2.517	−1.534	**−8.281**
Maiduguri	−0.021	**0.118**	**−0.059**	**0.278**	**0.175**	**−0.015**	**1.296**	0.146	**0.038**	**2.848**	1.648	**6.122**
Maine-Soroa	−0.061	**0.359**	**−0.388**	**0.555**	**0.556**	**−0.029**	0.091	0.078	0.015	−0.227	−0.315	**2.413**
Nguru	**−0.094**	**0.381**	**−0.195**	**0.220**	**0.625**	0.002	−0.032	0.476	−0.018	−0.270	−0.345	1.507
Potiskum	**0.269**	**0.337**	**−0.335**	**0.016**	**0.858**	**−0.029**	0.579	**−1.566**	0.037	**4.148**	0.330	**13.584**
Zinder	**0.170**	**0.331**	**−0.098**	**0.100**	**0.594**	−0.004	−0.078	−0.386	0.004	−0.843	−0.489	4.524

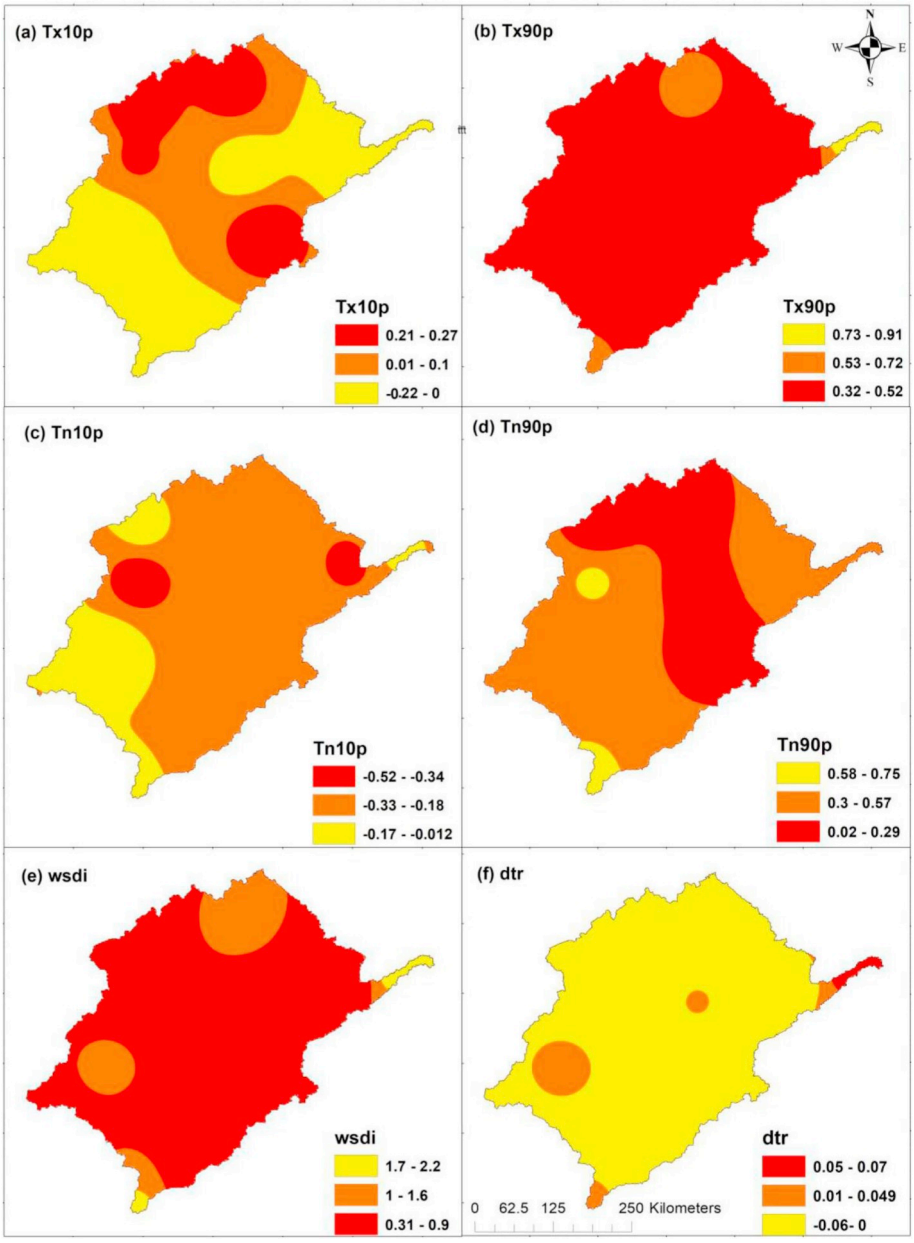

Fig. 2. Spatial trends in temperature indices for the validation period between 1979 and 2005 of: (a) Cool day frequency (%/year), (b) Warm day frequency (%/year), (c) Cool night frequency (%/year), (d) Warm night frequency (%/year), (e) Warm spells duration (days/year), and (f) Diurnal temperature range (^{0}C/year).

and warm night frequencies have statistically significant positive trends for all stations. Warm spells trend increase significantly in all stations. The diurnal temperature range trend varies between −0.08 and 0.09 °C/year with most stations having significant negative trends which indicates an increase in both maximum and minimum temperature with the minimum temperature having a greater rate of warming.

Fig. 2 shows the spatial trends in temperature indices for the validation period between 1979 and 2005. The result shows a decreasing trend of cool night frequency, cool day frequency and diurnal temperature range in most parts of the basin while the warm day frequency, warm night frequency and warm spells indicator, all having increasing trends. To test the ability of the bias-corrected CORDEX data to reproduce the spatial trends of the temperature indices, the spatial trend of the bias-corrected CORDEX data has been analysed between 1979 and 2005 (Fig. 3). The result shows a similar trend with the historical temperature indices for the validation period, however, with different magnitudes. For example, Figs. 2a and 3a show that the trend for cool day frequency for the validation period and bias-corrected CORDEX varies from −0.22–0.27%/year and from 0.35 to 0.32%/year respectively. The spatial patterns for both figures also show the negative trends (−0.35 to 0.00%/year) being recorded at the north-eastern and

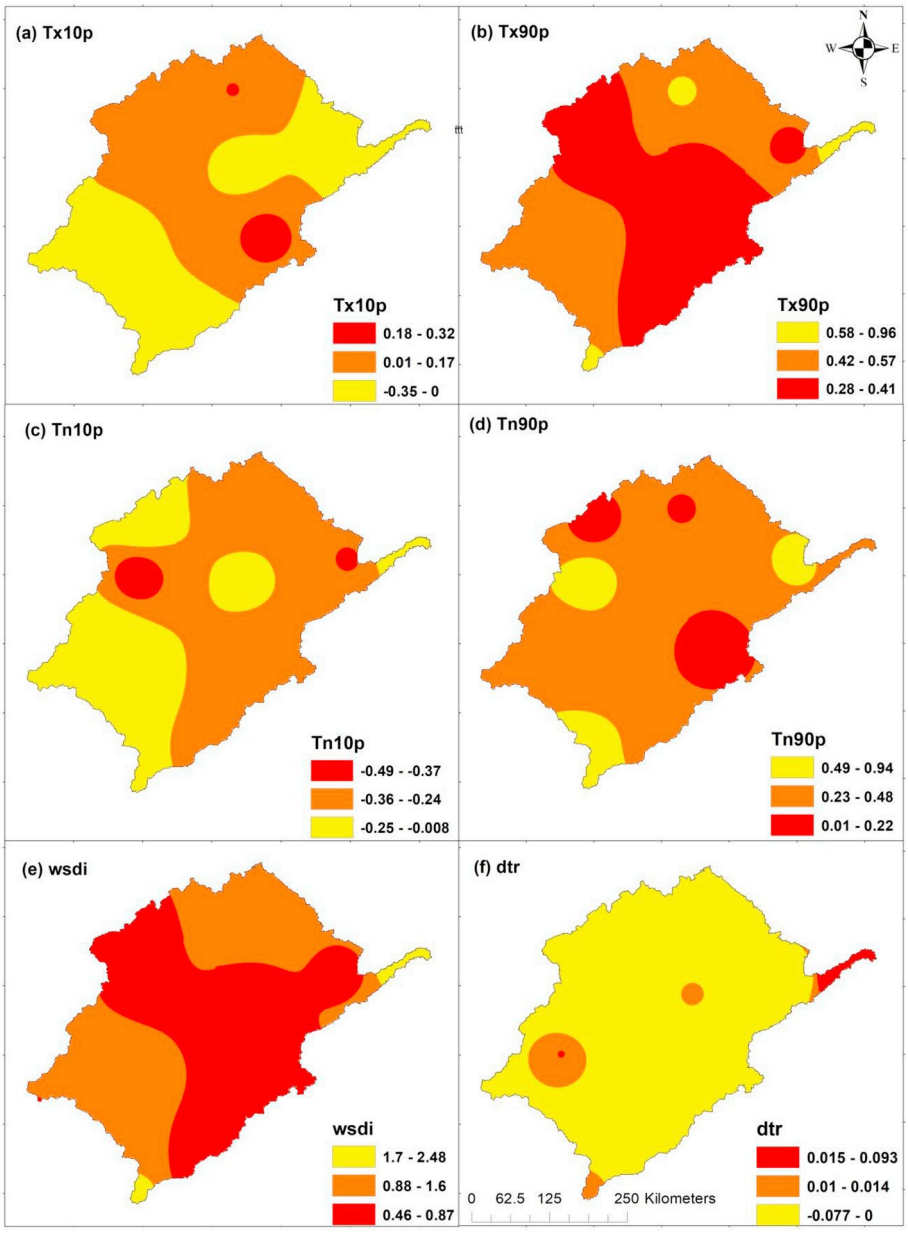

Fig. 3. Spatial trends in temperature indices for bias corrected CORDEX historical period between 1979 and 2005 of: (a) Cool day frequency (%/year), (b) Warm day frequency (%/year), (c) Cool night frequency (%/year), (d) Warm night frequency (%/year), (e) Warm spells duration (days/year), and (f) Diurnal temperature range (^{0}C/year).

Table 4
Number of stations with significant and non-significant trends for observed historical period (1971–2017).

(a) Temperature indices			(b) Rainfall indices		
Indices	Significant positive Trend	Significant negative Trend	Indices	Significant positive Trend	Non-significant negative Trend
tx10p	2	7	rx5day	5	3
tx90p	14	0	cdd	2	0
tn10p	0	10	cwd	2	4
tn90p	12	0	r95p	6	0
wsdi	14	0	r99p	3	0
dtr	1	7	prcptot	7	2

south-western parts of the basin.

In Table 4a, the number of stations with significant and non-significant trend in temperature indices is analysed. This shows that five, ten and seven stations observed significant negative trends in cool day frequency, cool night frequency and diurnal temperature range respectively while fourteen, twelve and fourteen stations observed significant positive trends in warm day frequency, warm night frequency and warm spells duration respectively.

4.2. Precipitation indices

Unlike temperature, the variations in the trend of rainfall are dependent on local and regional characteristics. The analysis of trend for the observed historical period (1971–2017) shows mixed trend in the 5-day cumulative rainfall (Table 3) with significant increasing trend in five stations and significant decreasing trend in one station (Table 4b).

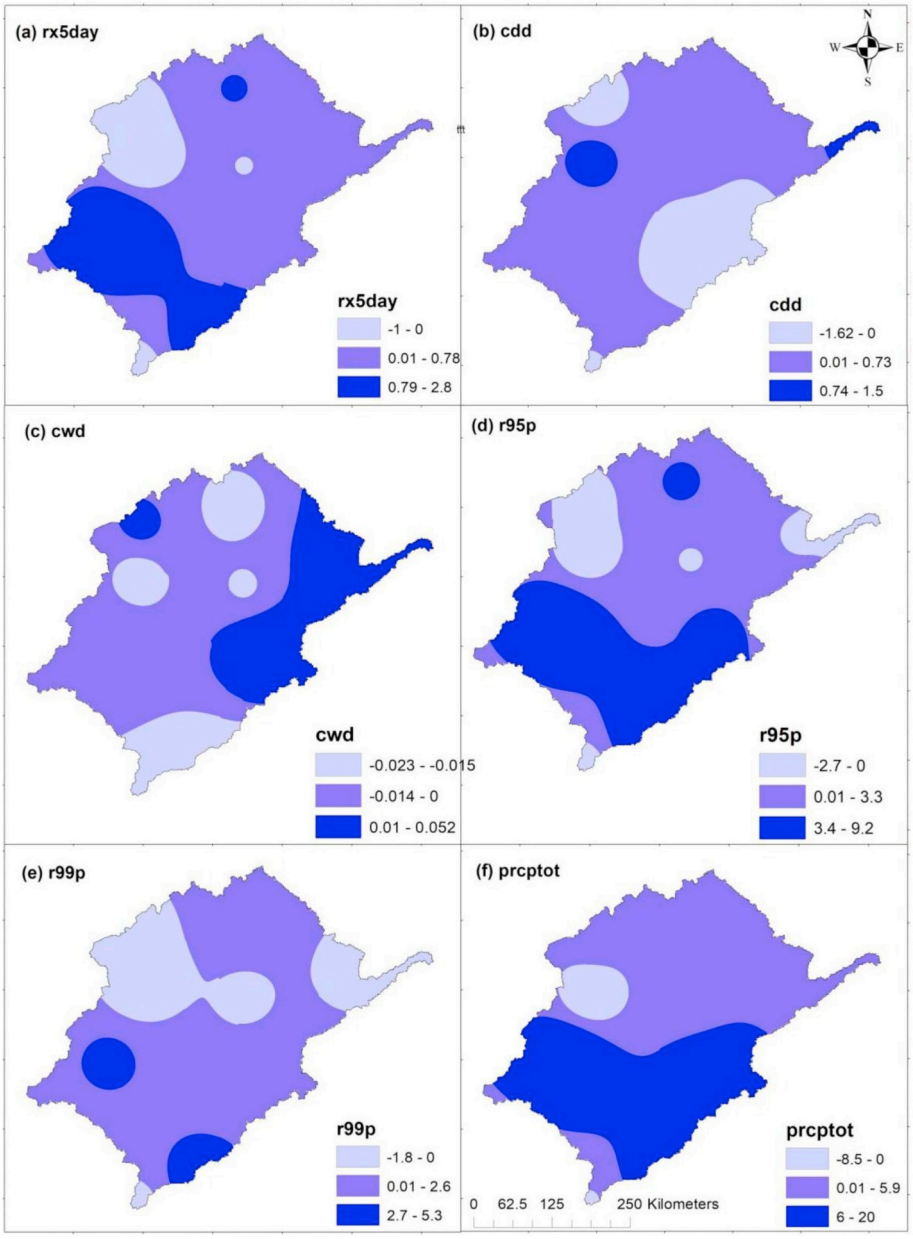

Fig. 4. Spatial trends in precipitation indices for the validation period between 1979 and 2005 of: (a) Maximum 5-day precipitation (mm/year), (b) Consecutive dry days (days/year), (c) Consecutive wet days (days/year), (d) Very wet days (mm//year), (e) Extremely wet days (mm/year), and (f) Annual total rainfall (mm/year).

There are increasing trends in the number of consecutive dry days except for Jos, Potiskum and Zinder with negative trends (Table 3; Table 4b). The consecutive wet days also have a decreasing trend in seven stations and an increasing trend in the other seven stations. There are mixed trends in the frequency of very wet days and extremely wet days. Annual total precipitation has positive trends in eleven stations with one station having significant negative trend with values varying between −8.28 and 19.39 mm/year.

The spatial patterns of the trends in the validation period and bias-corrected CORDEX data between 1979 and 2005 (Figs. 4 and 5) show an increasing trend of maximum 5-days rainfall, consecutive dry days, very wet days and annual total rainfall while the consecutive wet days and extremely wet days had decreasing trends in most parts of the basin.

Table 5 presents the validation results of the bias-corrected CORDEX and raw CORDEX for the entire basin. The bias-corrected CORDEX performed better than the raw CORDEX in reproducing the trends of the climate indices for the validation period between 1979 and 2005. It was also able to capture the significant observed direction and magnitude in the indices. This provides the basis and confidence in using the bias correction method for future projections.

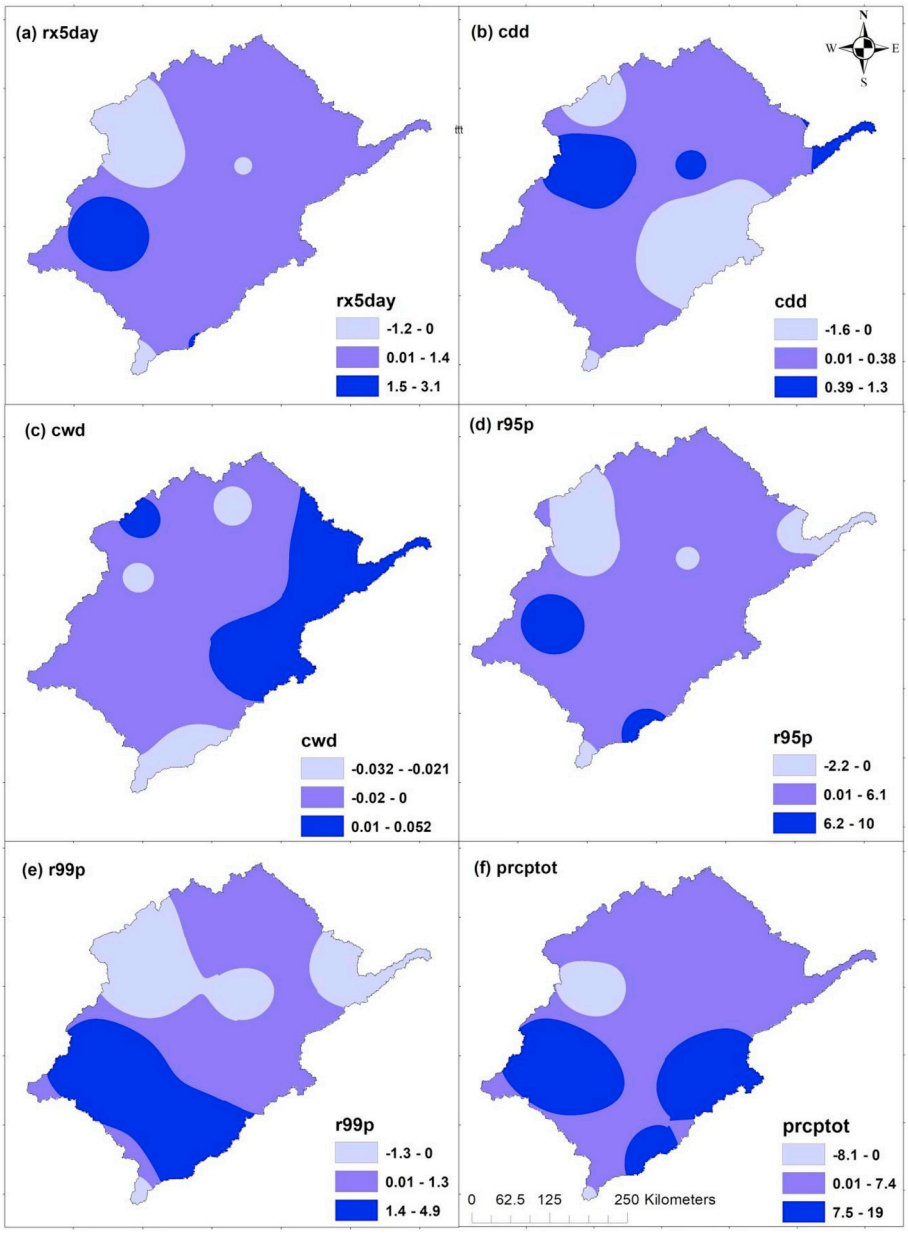

Fig. 5. Spatial trends in precipitation indices for bias corrected CORDEX historical period between 1979 and 2005 of: (a) Maximum 5-day precipitation (mm/year), (b) Consecutive dry days (days/year), (c) Consecutive wet days (days/year), (d) Very wet days (mm/year), (e) Extremely wet days (mm/year), and (f) Annual total rainfall (mm/year).

4.3. Projection

Table A.2 presents the results of climate indices over the basin under two representative concentration pathways (RCP4.5 and RCP 8.5) projections for global warming for two-time slices. The time slices are given near future (2020–2050) and far future (2060–2090).

4.3.1. Temperature indices trend under RCP 4.5

For the near future (Table A.2 a), the trends in cool day frequency, cool night frequency and diurnal temperature range are seen to be significantly decreasing in all stations except for three stations with non-significant negative trend in diurnal temperature range. The trend in warm day frequency, warm night frequency and warm spells duration are seen to be significantly positive in all stations except for two stations with non-significant positive trend in warm night frequency.

The spatial trend pattern (Fig. 6) shows a decreasing trend of cool day frequency, cool night frequency and diurnal temperature range for the entire basin while the warm day frequency, warm night frequency and warm spell duration exhibited increasing trends. High magnitudes of negative trends in cold night frequency decreases towards the south-

Table 5
Basin-scale trend of indices for validation period from observed data, bias-corrected CORDEX and raw CORDEX between 1979 and 2005. Bold values represent significant change in trend.

	Temperature Indices						Rainfall Indices					
	tx10p	tx90p	tn10p	tn90p	wsdi	dtr	rx5day	cdd	cwd	r95p	r99p	prcptot
Validation period												
Slope	**−0.30**	**0.35**	**−0.72**	**0.40**	0.18	0.01	**0.60**	0.34	**0.85**	**4.94**	1.27	**11.00**
Bias-Corrected CORDEX												
Slope	**−0.32**	**0.21**	**−0.73**	**0.37**	0.26	0.01	**0.50**	0.42	**0.66**	**3.44**	1.02	**10.24**
SD	0.01	0.10	0.01	0.02	0.06	0.00	0.07	0.06	0.13	1.06	0.18	0.54
RMSE	0.02	0.14	0.01	0.03	0.08	0.00	0.10	0.08	0.19	1.50	0.25	0.76
MSE	0.00	0.02	0.00	0.00	0.01	0.00	0.01	0.01	0.04	2.25	0.06	0.58
PBIAS	6.7	−40.00	1.40	−7.50	44.40	0.00	−16.70	23.50	−22.40	−30.40	−19.70	−6.90
Raw CORDEX												
Slope	**−0.41**	**0.60**	**−0.74**	**1.13**	**1.25**	**−0.01**	−0.01	**1.77**	0.02	1.41	0.10	**1.67**
SD	0.08	0.18	0.02	0.51	0.76	0.01	0.43	1.01	0.58	2.49	0.83	6.60
RMSE	0.11	0.25	0.02	0.73	1.07	0.02	0.61	1.43	0.83	3.53	1.17	9.33
MSE	0.01	0.06	0.00	0.53	1.15	0.00	0.37	2.05	0.69	12.46	1.37	87.05
PBIAS	36.70	71.40	2.80	182.50	594.4	−200.00	−101.70	420.6	−97.60	−71.50	−92.10	−84.80

SD is the standard deviation, RMSE is the root mean square error, MSE is the mean square error and PBIAS is the percentage bias.

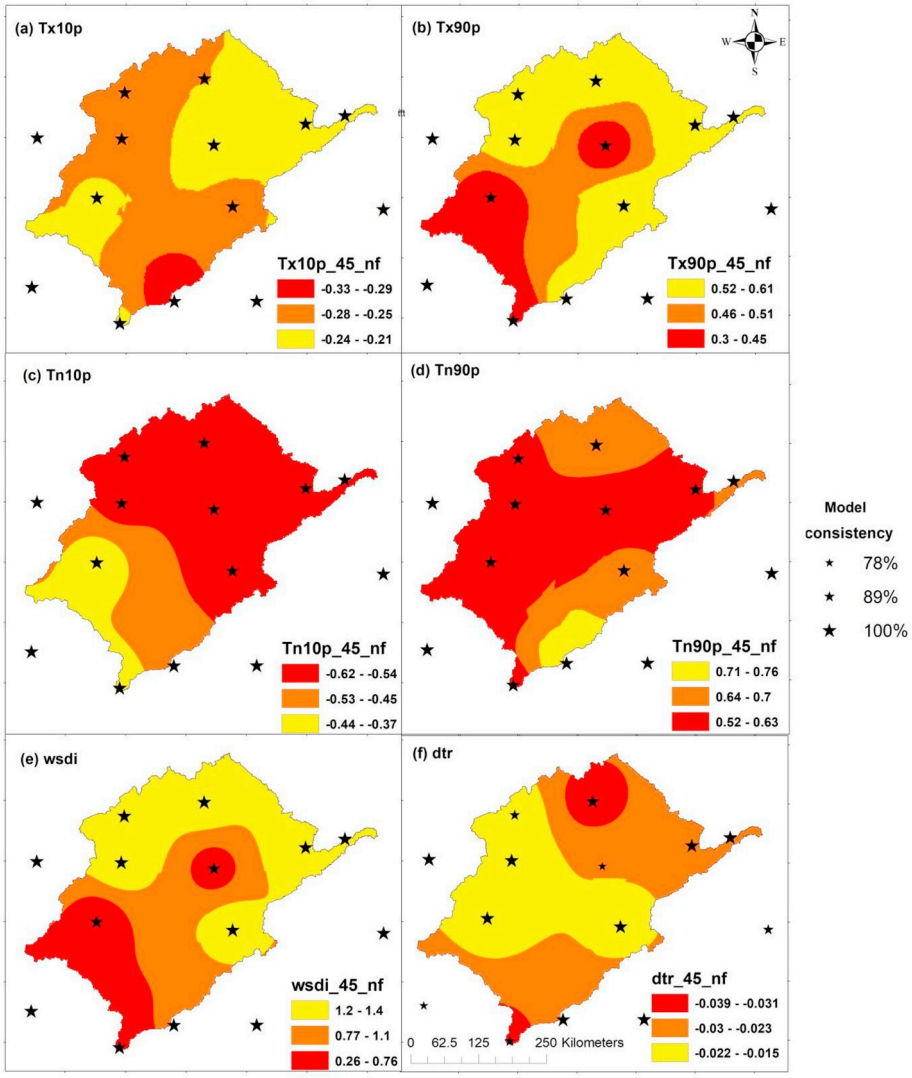

Fig. 6. Spatial trends in temperature indices for the near future (202–2050) under RCP 4.5 (a) Cool day frequency (%/year), (b) Warm day frequency (%/year), (c) Cool night frequency (%/year), (d) Warm night frequency (%/year), (e) Warm spells duration (days/year), and (f) Diurnal temperature range (^{0}C/year).

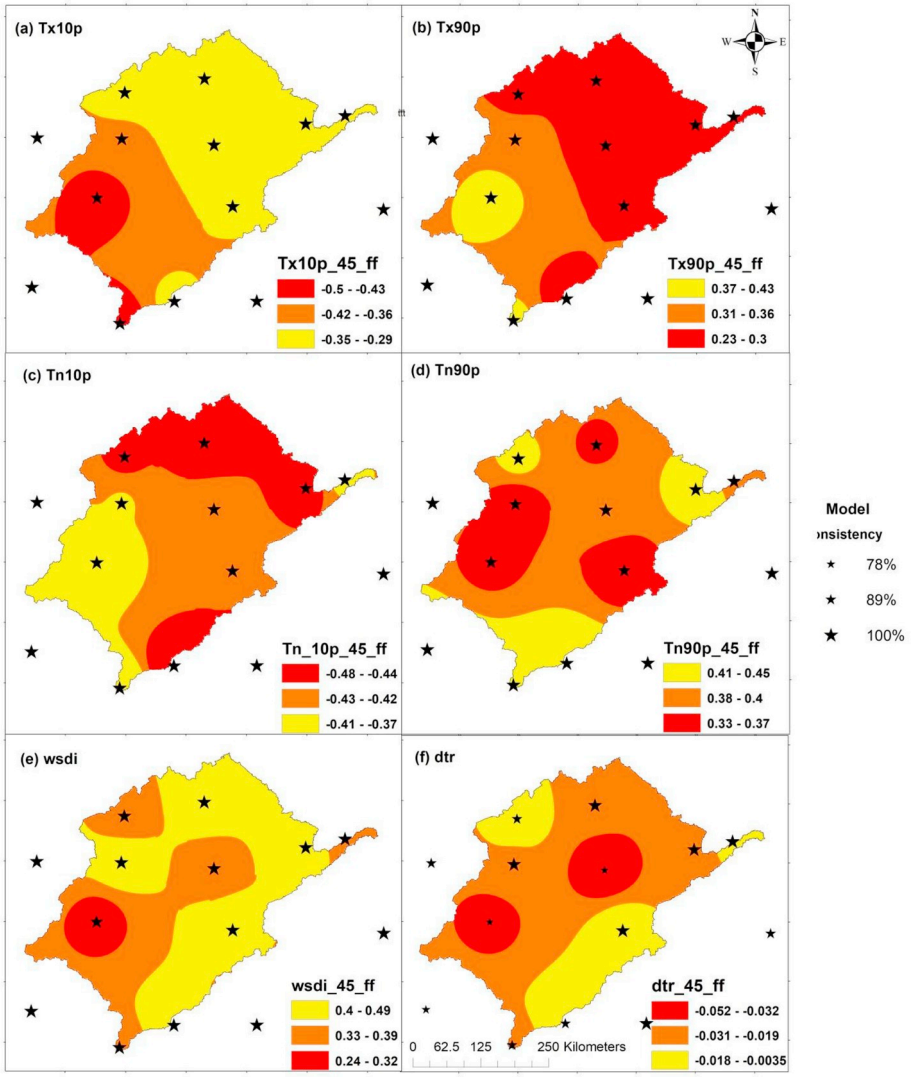

Fig. 7. Spatial trends in temperature indices for the far future (2060–2090) under RCP 4.5 (a) Cool day frequency (%/year), (b) Warm day frequency (%/year), (c) Cool night frequency (%/year), (d) Warm night frequency (%/year), (e) Warm spells duration (days/year), and (f) Diurnal temperature range (^{0}C/year).

western part of the basin while the positive trends in warm spell duration also decrease towards the south-western part. The consistency rate of the eight bias corrected models and the ensemble mean (nine models altogether) shows maximum consistency (100%) for all temperature indices except for diurnal temperature range with model consistency between 78% and 100%.

For the far future (Table A.2 b), cool day frequency and cool night frequency still exhibit significant negative trend in for all stations in the basin. However, diurnal temperature range both significant and non-significant negative trend although with some stations like Bauchi, Gombe, Potiskum and Zinder having no trend. Positive trend in warm day and warm night frequencies is evident in all stations.

The spatial trends (Fig. 7) reveals that the highest negative trend in cool night frequency (−0.44 to −0.48%/year) while the lowest negative trend in cool night frequency (−0.37 to −0.41%/year) is also seen at the south-western side of the basin. The highest positive trend for warm night frequency (0.41–0.45% per year) is also seen at the southern and north-eastern part of the basin. The warm spell duration possesses high trend values (0.42–0.49 days/year) in most parts of the basin. This trend gradually decreases towards the south-western part of the basin. The model consistency varies between 78% and 100% for diurnal temperature range while it maintains a maximum consistency for other temperature indices.

4.3.2. *Temperature indices trend under RCP 8.5*

Results of near future analysis under RCP 8.5 (Table A.2 c) show significant negative trends in cool night frequency, cool day frequency and diurnal temperature range for all stations while all stations exhibited significant increasing trend in warm day frequency, warm night frequency and warm spell duration.

The spatial trend pattern (Fig. 8) shows that highest values of negative trend in cool day frequency (−0.56 to −0.64%/year) is recorded in the south-western sector of the basin while the highest values for negative trend in cool night frequency (−0.71 to −0.81%/year) is seen in most parts of the basin. High positive trend in warm spell duration (0.88–1.60 days/year) is seen in most parts of the basin. The model consistency varies between 89% and 100% for diurnal temperature range while it retains a 100% consistency for other

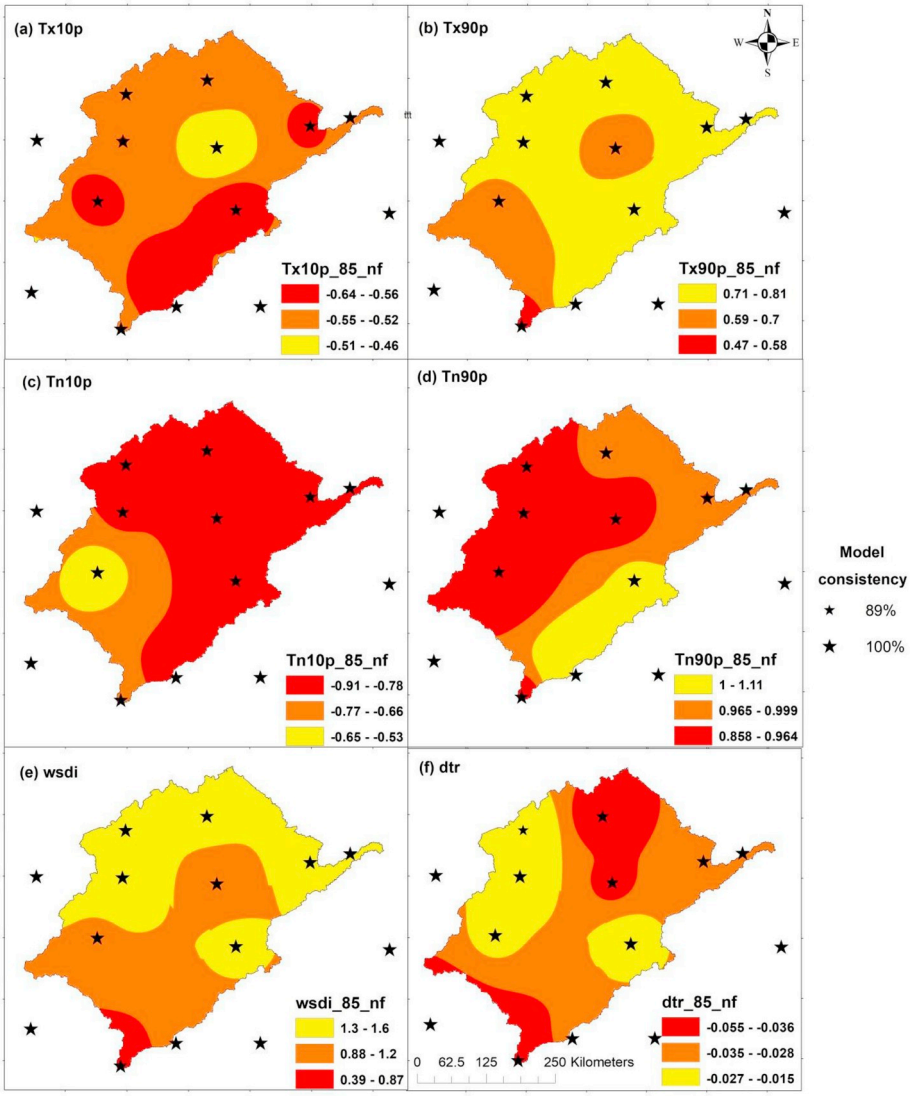

Fig. 8. Spatial trends in temperature indices for the near future (2020–2050) under RCP 8.5 (a) Cool day frequency (%/year), (b) Warm day frequency (%/year), (c) Cool night frequency (%/year), (d) Warm night frequency (%/year), (e) Warm spells duration (days/year), and (f) Diurnal temperature range (^{0}C/year).

temperature indices.

For far future analysis (Table A.2 d), there is a negative trend in the diurnal temperature ranges and cool night and cool day frequencies. There is a positive trend in warm spell duration and warm day and warm night frequencies. The spatial pattern of the trend (Fig. 9) shows that negative trend in cold day and cold night frequencies increases towards the southern part of the basin while the positive trends in warm day and warm night frequencies also increase towards the southern part. The warm spell duration increases towards the northern part of the basin. The magnitude of trend analysis comparison of the historical extremes with RCP 4.5 both for near and far future shows an increasing magnitude of the temperature extreme events.

4.3.3. Precipitation indices trend under RCP 4.5

All precipitation indices except consecutive dry days are observed to have negative trends in the near future with the highest negative trend of −39.02 mm/year in annual total rainfall (Table A.2.a). The negative trends in annual total rainfall are statistically significant in Bauchi, Gombe, Nguru and Potiskum stations. Negative trends are observed in maximum 5-days rainfall, consecutive wet days and annual total rainfall for near future time slice. However, some of these negative trends are not statistically significant. The consecutive dry days had all positive trends except for the negative trends at Diffa, Magaria and Zinder stations. The spatial trend (Fig. 10) also suggested an overall negative trend in maximum 5-days rainfall, consecutive wet days, wet days, very wet days and annual total precipitation across the basin. However, the pattern of trend differs across the basin. For example, negative trend in maximum 5-days rainfall, consecutive wet days, very wet days, extremely wet days and annual total precipitation increase towards the south-west, while the negative trend in consecutive dry days increases towards the north-western part of the basin. The model consistency varies between 78% and 100%.

For far future time slice, all trends turned positive for annual total rainfall, having the highest positive trend of 23.33 mm/year except for Goure Katsina and Zinder with negative trends of −1.67, −0.56 and −6.24 mm/year respectively. Nevertheless, other precipitation indices

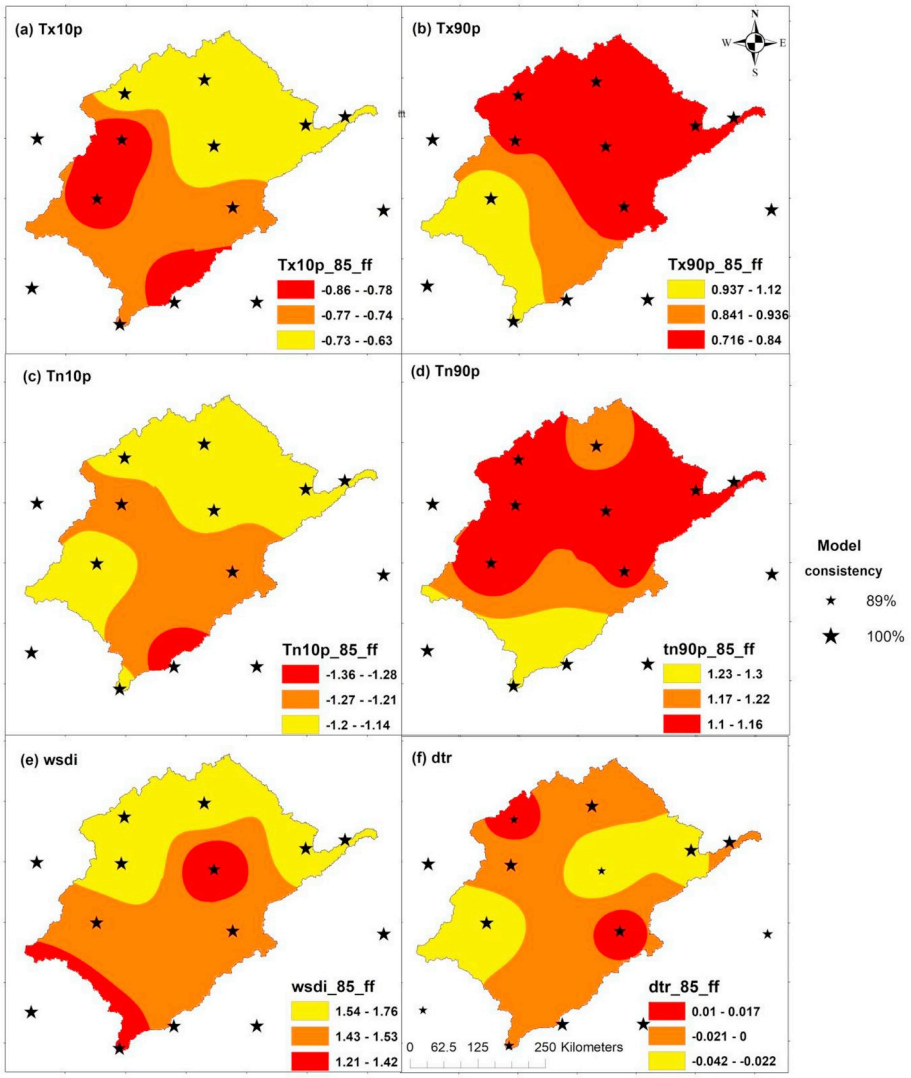

Fig. 9. Spatial trends in temperature indices for the far future (2060–2090) under RCP 8.5 (a) Cool day frequency (%/year), (b) Warm day frequency (%/year), (c) Cool night frequency (%/year), (d) Warm night frequency (%/year), (e) Warm spells duration (days/year), and (f) Diurnal temperature range (^{0}C/year).

have mixed positive and negative trends for the stations. The spatial trend (Fig. 11) shows that negative trends in precipitation indices are predominantly located at the north-western part of the basin except for consecutive dry days. The model consistency varies between 56% and 100%. The comparison of magnitude of trend for the historical and RCP 4.5 extremes shows a mixed pattern. For example, maximum 5-days rainfall, consecutive wet days, extremely wet days and annual total rainfall all had negative magnitudes while consecutive dry days had mixed magnitude for all stations while very wet days had a negative magnitude except for Zinder station under RCP 4.5 for near future. For far future, there was generally a mixed magnitude of trend for all precipitation indices. Overall, there is a drying trend in the basin.

4.3.4. Precipitation indices trend under RCP 8.5

Under RCP 8.5 for near future (Table A.2 c), all precipitation indices show negative trends except for the consecutive dry days with some positive trends. The highest negative trend of −36.46 mm/year was recorded in annual total rainfall. The negative trends in annual total rainfall are significant in all stations within the basin. Maximum 5-days rainfall, consecutive wet days, very wet days and extremely wet days all have negative trends for every station, although with some degree of significance and non-significance. The spatial trends (Fig. 12) in annual total rainfall, very wet days, extremely wet days and consecutive wet days all decreases towards the southern part of the basin.

For far future (Table A.2 d), all precipitation indices trend are positive except for consecutive wet days with a not-significant negative trend at Goure. The highest positive trend (48.35 mm/year) is reported for annual total rainfall at Jos. There are mixed occurrences of both significant and not-significant trends for this time slice. The spatial trend (Fig. 13) shows that all precipitation indices show increment towards the southern part of the basin except for consecutive dry days which shows an increment towards the north-western part of the basin.

The magnitude of trend comparison between historical extremes and RCP 8.5 shows a mixed change in the magnitude of the rainfall extreme events. For near future, all precipitation indices had negative magnitudes except consecutive dry days with a mixed magnitude. For far future scenarios, maximum 5-days rainfall had negative trend except for Kano, consecutive dry days had positive magnitude except for

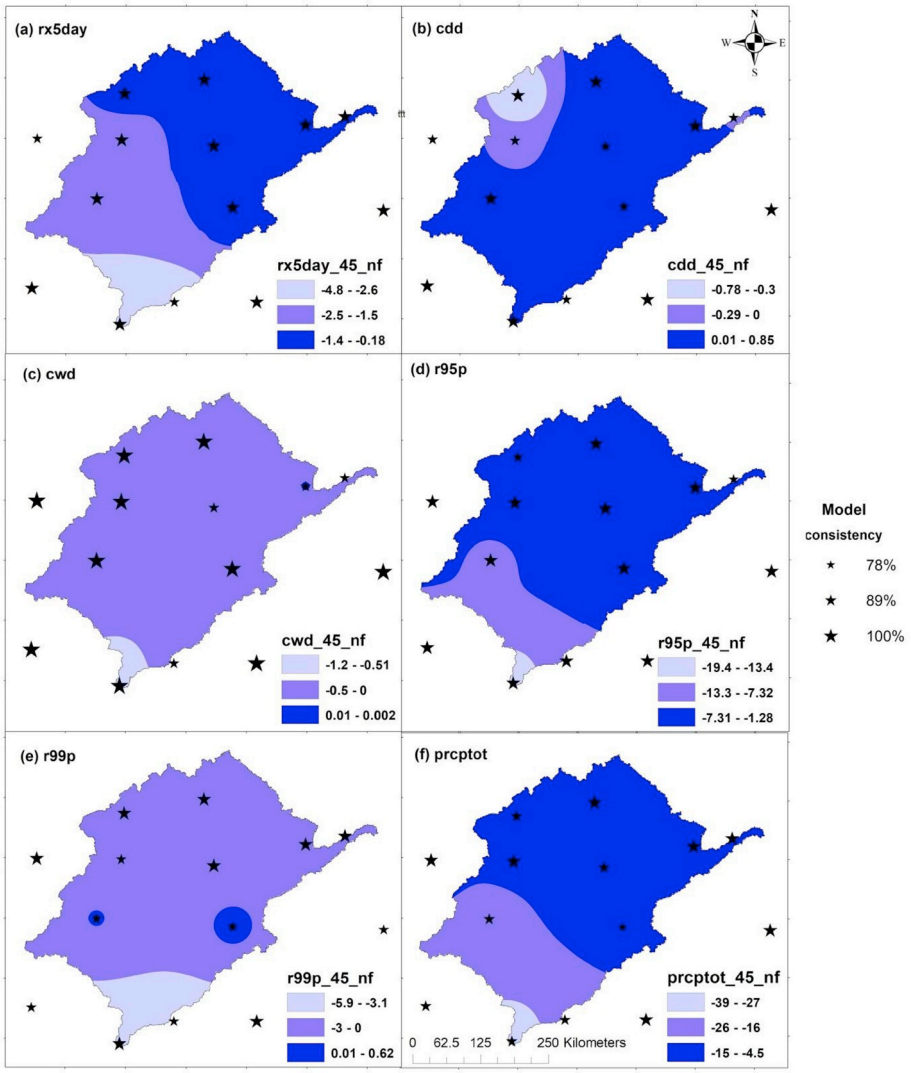

Fig. 10. Spatial trends in precipitation indices for the near future (2020–2050) under RCP 4.5 (a) Maximum 5-day precipitation (mm/year), (b) Consecutive dry days (days/year), (c) Consecutive wet days (days/year), (d) Very wet days (mm/year), (e) Extremely wet days (mm/year), and (f) Annual total rainfall (mm/year).

Maiduguri, consecutive wet days had positive magnitude except for Goure, very wet days had positive magnitude except for Goure and Kano, extremely wet days had positive magnitude except for Bauchi and Kano and annual total rainfall had positive magnitude except for Kano.

In general, there is no global pattern in of rainfall extreme trends between RCP 4.5 and 8.5 because the pattern of magnitude and trend depends on the location of the station. However, most of the indices had an increasing magnitude from RCP 4.5 to 8.5.

Figures A.1 and A.2. further quantifies the uncertainties associated with the model projection. For example, in figure A.1, all models seem to have similar range for extremely wet days for most part of the projection period for Maine station while this is not same for diurnal temperature range. Figures for other stations are presented in Adeyeri et al. (2018).

5. Discussion

In this study, climate extreme indices in the Komadugu-Yobe basin, Lake Chad region were analysed. For the observed historical period, the temperature indices show significant warming trends for all stations while the precipitation indices have no uniform trend. To validate the ability of the ensemble climate model to capture present-day extremes and their trends, we analysed the results from the raw CORDEX, bias-corrected CORDEX and validation period from observed data outputs. The results show a similar pattern of extreme climate indices over the basin. However, the raw CORDEX overestimated the trend of most indices while the significant magnitude was not captured. The bias-corrected CORDEX performed better as it was able to capture both pattern and significant magnitude in trends.

The temperature indices considered show a significant warming trend in the basin. This result confounds with previous studies in other regions of Africa. For example, Ly et al. (2013) reported warming trend throughout the Sahel between 1960 and 2010. Gbode et al. (2018) reported a significant increase in the frequencies of warm days and warm night, warm spell duration over three climatic zones in Nigeria between 1971 and 2013. Abatan et al. (2017a) also reported a warming trend over Nigeria between 1971 and 2012 with warming most pronounced in southern Nigeria. Our results in this study are consistent with these findings. However, Abatan et al. (2017a) observed most significant warming trends in some stations located in the coastal areas.

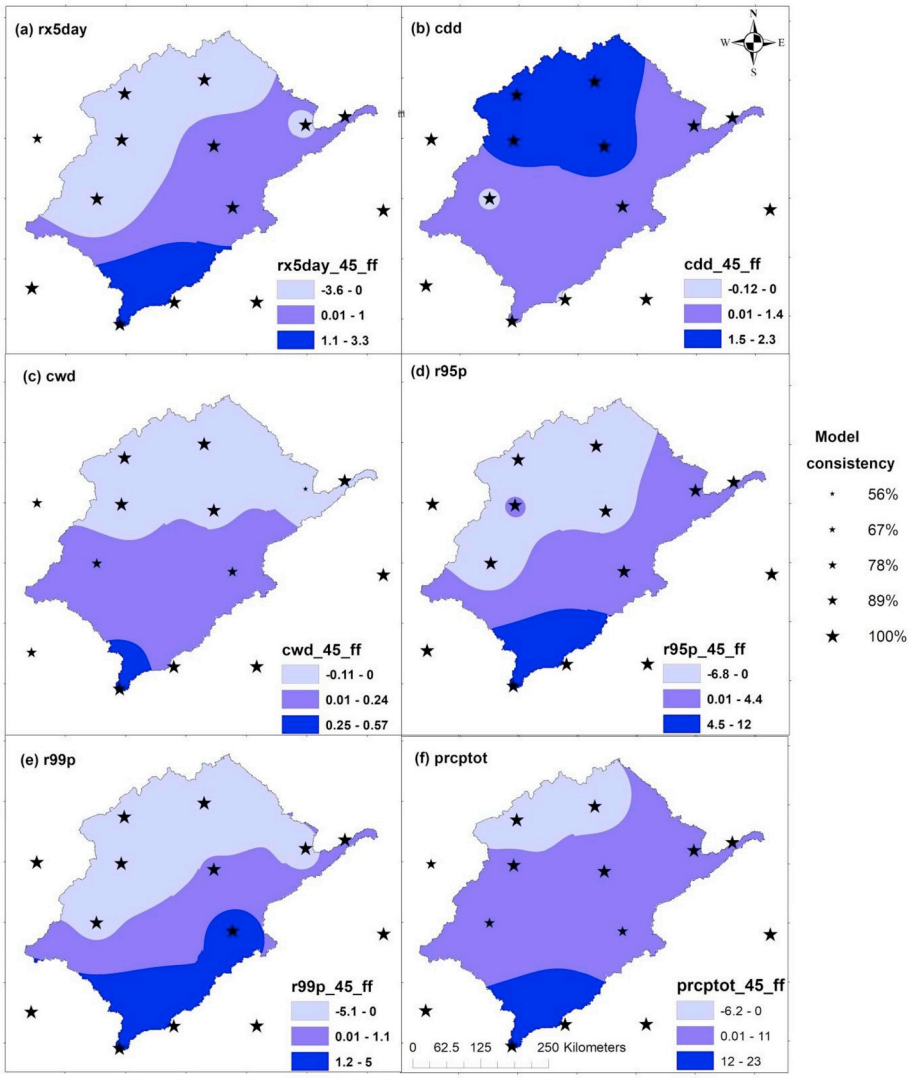

Fig. 11. Spatial trends in precipitation indices for the far future (2060–2090) under RCP 4.5 (a) Maximum 5-day precipitation (mm/year), (b) Consecutive dry days (days/year), (c) Consecutive wet days (days/year), (d) Very wet days (mm/year), (e) Extremely wet days (mm/year), and (f) Annual total rainfall (mm/year).

Though, there was no significant difference in the coastal and inland stations in our study area which may be attributed to the reduced ocean-land temperature gradient that characterised the monsoon region as reported by Ly et al. (2013). The increase in the warm spell frequencies could be attributed to the increase in greenhouse gases concentration in the atmosphere which results in global warming. The negative trend of the diurnal temperature range in the study area could be caused by a faster warming of the minimum temperature even though there was an increase in both maximum and minimum temperatures (Ly et al., 2013). The projected increase in warm spell and the overall warming of the stations in the basin for near and far future under RCP4.5 and RCP8.5 is an indication that the future normal temperature may become more severe than the past if mitigation measures are not in place to abate the warming.

For precipitation indices, the increase in annual total rainfall in the basin is consistent with Lebel and Ali (2009) which might have been caused by the Sahelian rainfall recovery (Thompson and Polet, 2000). The significant increasing trend of very wet days and extremely wet days observed in the study area is in line with the findings of Sarr (2011) who reported an increase in the frequency of extreme rainfall events in the Sahel. However, it should be noted that despite the increasing frequency of extreme rainfall events, there was also an increasing trend in consecutive dry days with a decreasing consecutive wet day.

Due to the spatial variability of precipitation, the projected precipitation indices appear to follow different trends at different time slices under the two RCPs. For example, all annual total rainfall, extremely wet days, very wet days and maximum 5-day rainfall follow a negative trend for near future although not statistically significant for all stations under RCP4.5 and 8.5 near future scenarios but turned majorly positive for all indices under both scenarios for far future depicting a more intense extreme event in the future. This result is consistent with Abiodun et al. (2017) who stated that the result of GCM projections showed a likely increase in extreme precipitation events over West Africa. Abiodun et al. (2017) also documented a decrease in projected wet days frequency and annual total precipitation over Maputo between 2081 and 2100 under the RCP8.5 scenario. Same authors also noted an increase in annual total precipitation over Lagos between

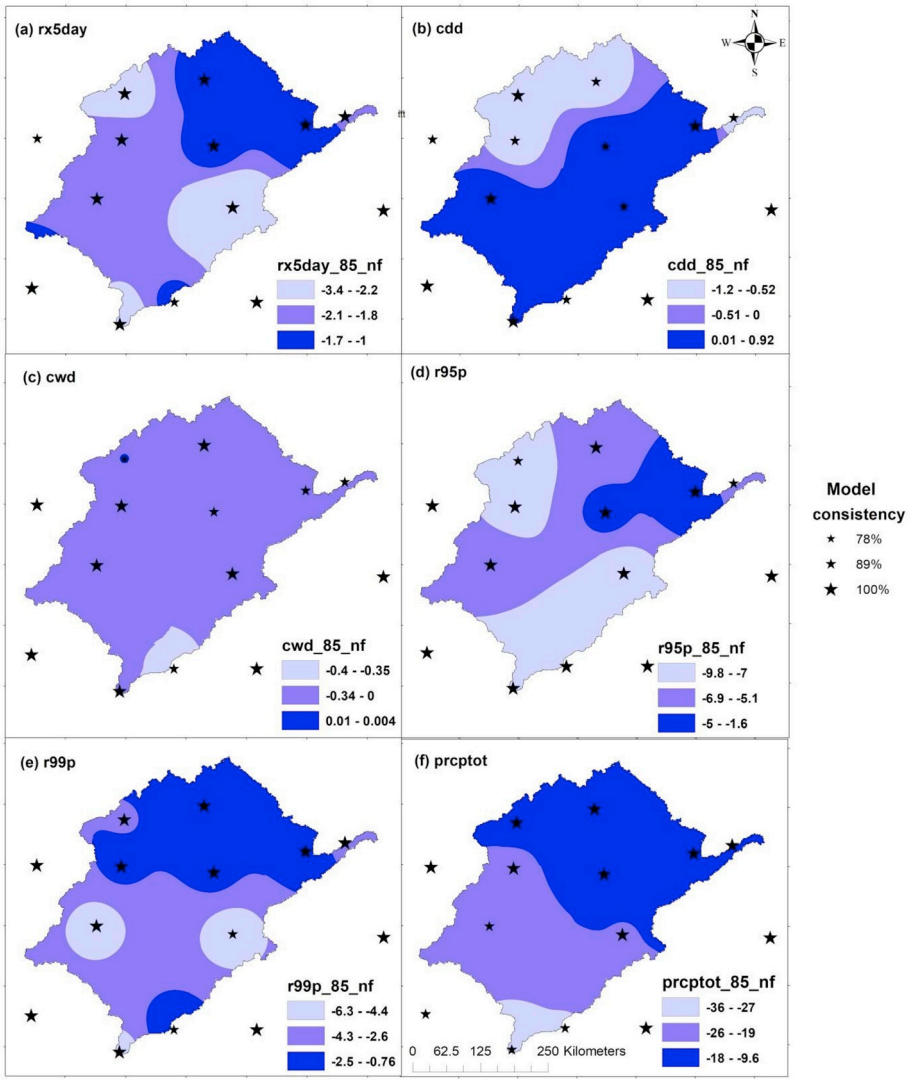

Fig. 12. Spatial trends in precipitation indices for the near future (2020–2050) under RCP 8.5 (a) Maximum 5-day precipitation (mm/year), (b) Consecutive dry days (days/year), (c) Consecutive wet days (days/year), (d) Very wet days (mm/year), (e) Extremely wet days (mm/year), and (f) Annual total rainfall (mm/year).

2081 and 2100 under both RCP scenarios.

Whilst the projected decrease in the frequency and intensity of extreme precipitation especially over Kano for near future under both RCP scenarios will inevitably affect the levels of water in the two dams in the Kano (Tiga and Challawa dams), and also affect the water used for irrigation purposes in the Sahelian basin, the far future slices under the two RCP scenarios showed a projected increase in the frequency and intensity of extreme precipitation which suggests flooding as well as more water for hydro-electricity and irrigation, hence, more water supply to the drying Lake Chad. The projected increase in dry spells could reduce agricultural productivity, food security and a potential pressure on the available freshwater resources in the basin (Abiodun et al., 2017).

Although, the uncertainties associated with climate change impact assessment on extreme indices cannot be under-emphasised. This includes GCM and RCM configurations and the RCP scenarios. However, in this study, the uncertainty range was minimized by analysing the model ensemble mean as seen in the comparison results of the CORDEX historical period with validation period.

6. Summary and conclusion

In order to understand the susceptibility of river basins to climate change, this study investigated the impact of climate change on climate extreme indices in the Komadugu-Yobe basin, Lake Chad region using homogenised observed stations' data for past climate extremes' characteristics and the ensemble mean of 8 bias-corrected CORDEX climate models for future projection of climate extremes under two RCP scenarios. The results show that there is a warming trend in temperature in the basin while the precipitation indices do not have uniform trend conformity as this depends on the precipitation index of concern.

Generally, over the entire basin, the magnitude of the trends of hot extremes was greater than the cold extremes which imply that the distributions of the warm extremity associated with the increasing daily temperature are more pronounced. The increased positive trends in total annual rainfall and corresponding positive trends in the intensity of wet events coincide with the positive trends of hot extremes which indicate the capacity of the warmer air to hold more moisture resulting in a prolonged low-level moisture convergence and possible occurrence

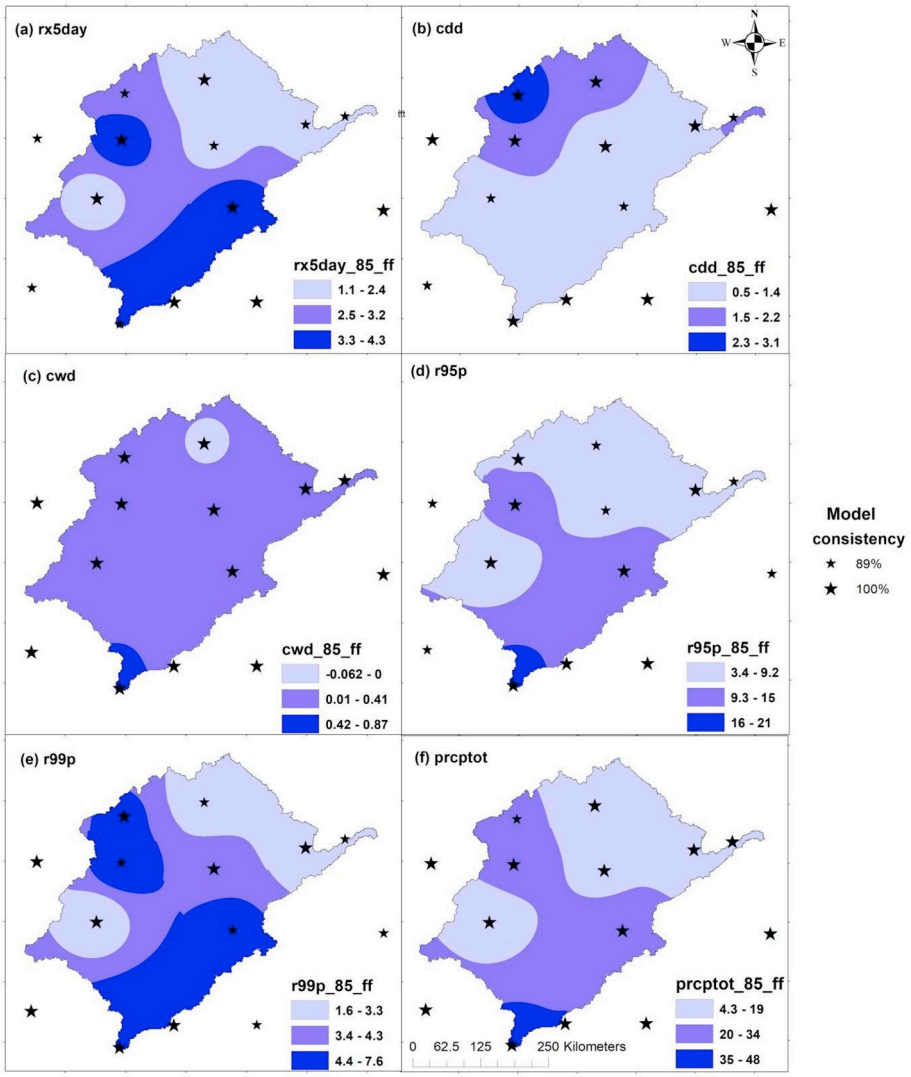

Fig. 13. Spatial trends in precipitation indices for the far future (2060–2090) under RCP 8.5 (a) Maximum 5-day precipitation (mm/year), (b) Consecutive dry days (days/year), (c) Consecutive wet days (days/year), (d) Very wet days (mm/year), (e) Extremely wet days (mm/year), and (f) Annual total rainfall (mm/year).

of storm activities in the region. Furthermore, the historical and future climate extreme characteristics revealed similar patterns of trends over the study area. However, the magnitude of the projected climate extremes, most importantly temperature, was continually greater in the latter years. These consistencies could be scaled with the RCP emission scenarios which have demonstrated a strong relationship between the anthropogenic GHG emissions and potential environmental impacts.

Future work must seek to explore and improve individual regional climate simulation, especially of precipitation, to reduce uncertainties and discrepancies in model outputs.

Therefore, the attempts in this study to characterize areas in the river basin with the potential risk of climate extreme events will serve as a useful resource for assessments of the potential impacts of climate change on human and ecosystems, and in turn enhance regional adaptation, hazard preparedness, planning strategies, and decision making.

Compliance with ethical standards

The Authors have read and understood the policy on declaration of interests and declare that we have no competing interests. This article does not contain any studies with human or animal subjects.

Conflict of interest

The authors have read and understood the policy on declaration of interests and declare that we have no competing interests. This article does not contain any studies with human or animal subjects.

Acknowledgement

The first author was supported by the doctoral scholarship from the Federal Ministry of Education and Research (BMBF) and West African Science Service Center on Climate Change and Adapted Land Use (WASCAL). The authors wish to acknowledge the Direction de la Meteorologie Nationale (DMN) of Niger Republic, the Nigeria Meteorological Agency (NiMet) and CORDEX for providing data used in this study. The Expert Team on Climate Change Detection Monitoring Indices (ETCCDMI) is also acknowledged for the provision of Rclimdex package used for the analysis of climate indices. We extend our thanks to Peter Domonkos for the provision of ACMANT package as well as the constructive discussions regarding the use of ACMANT. Our sincere appreciation also goes to Maurus Borne for the python scripts used for the analysis. The anonymous reviewers are acknowledged for their valuable comments and suggestions.

Appendix A. Supplementary data

Supplementary data to this article can be found online at https://doi.org/10.1016/j.wace.2019.100194.

Appendix

Table A.1
List of GCMs used as boundary conditions for the Rossby Centre Regional Atmospheric (RCA) model.

No	Modelling Centre	GCM
1	Canadian Centre for Climate Modelling and Analysis	CanESM2
2	Centre National de Recherches Météorologiques/Centre Européen de Recherche et Formation Avancée en Calcul Scientifique	CNRM-CM5
3	EC-EARTH consortium	EC-EARTH
4	NOAA Geophysical Fluid Dynamics Laboratory	GFDL-ESM2M
5	Met Office Hadley Centre	HadGEM2-ES
6	Atmosphere and Ocean Research Institute (The University of Tokyo), National Institute for Environmental Studies and Japan Agency for Marine-Earth Science and Technology	MIROC5
7	Max Planck Institute for Meteorology	MPI-ESM-LR
8	Norwegian Climate Centre	NorESM1-M

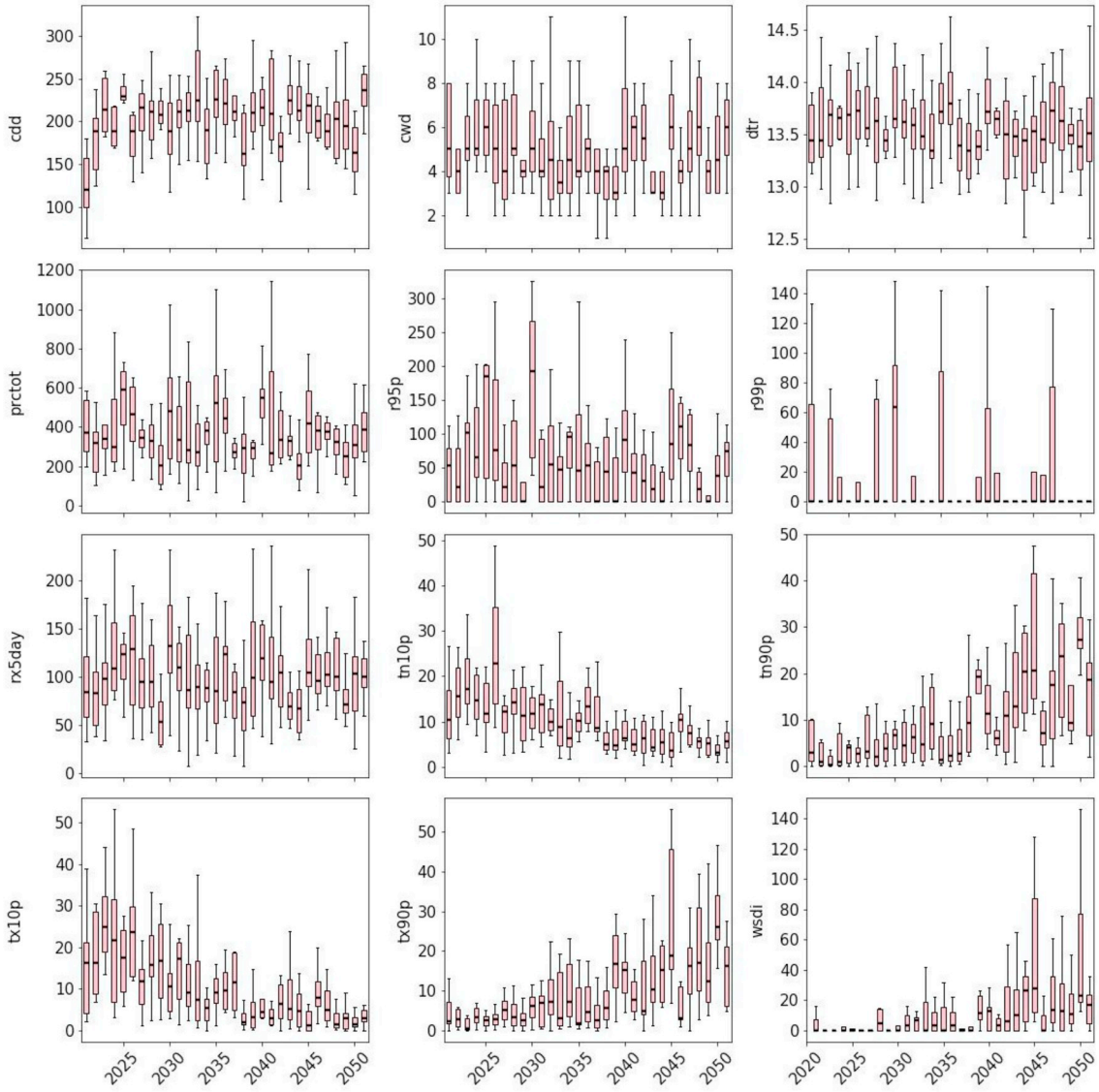

Figure A.1. Boxplot of climate indices consisting of 8 climate models with the ensemble mean for Maine station for the near future under RCP4.5 (2020–2050).

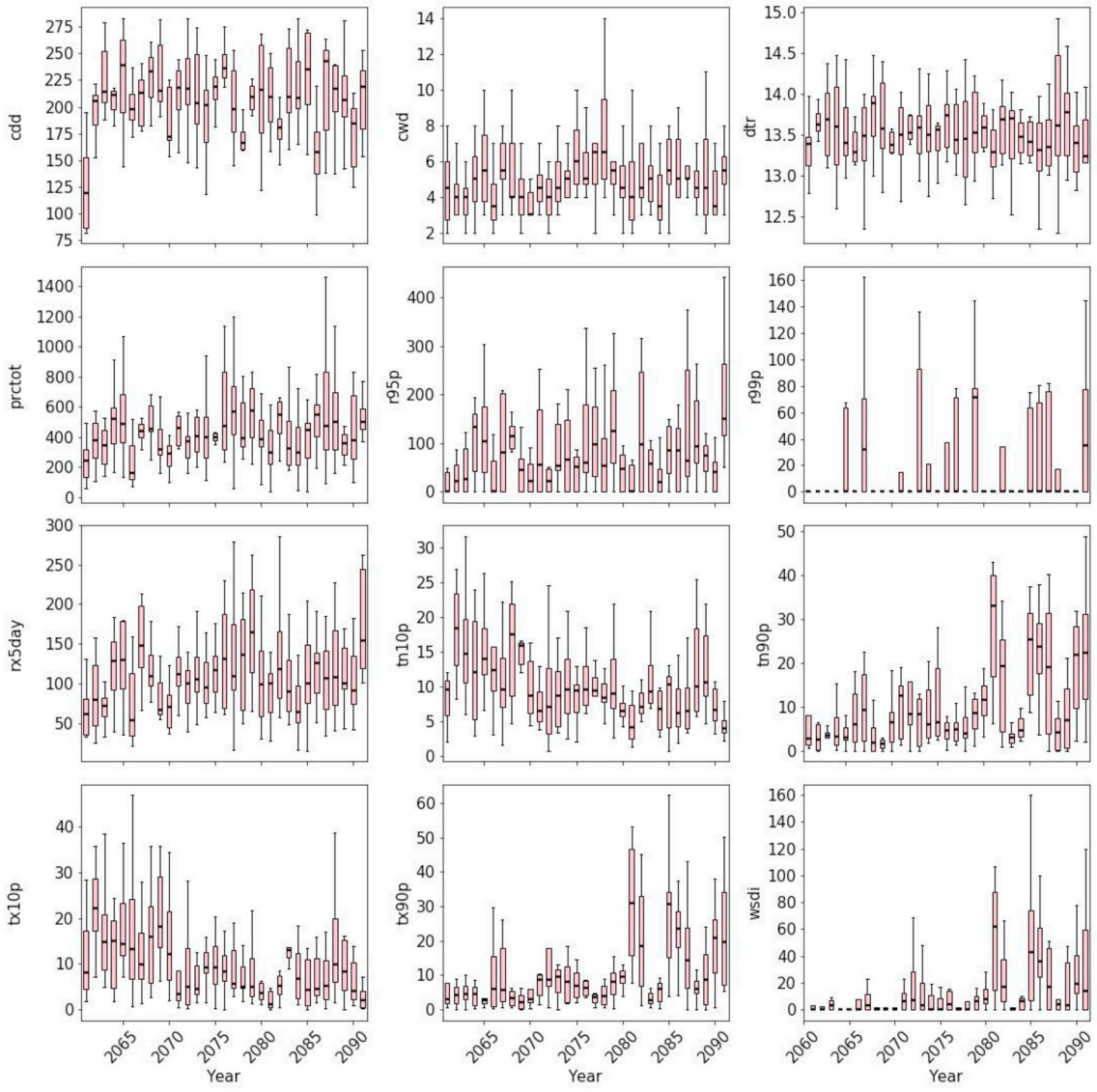

Figure A.2. Boxplot of climate indices consisting of 9 models for Maine station for the far future under RCP4.5 (2060–2090).

Table A.2
Trend in the projection of temperature and rainfall indices stations under RCP4.5 and RCP 8.5. Bold values represent significant changes. For more information about the location of the stations, please see Fig. 1.

a. Near future analysis at RCP4.5 (2020–2050)

Stations	Temperature Indices						Rainfall Indices					
	tx10p	tx90p	tn10p	tn90p	wsdi	dtr	rx5day	cdd	cwd	r95p	r99p	prcptot
Bauchi	**−0.33**	**0.58**	**−0.53**	**0.76**	**0.87**	**−0.02**	**−3.04**	0.68	**−0.19**	**−8.07**	**−5.31**	**−23.79**
Diffa	**−0.23**	**0.60**	**−0.56**	**0.65**	**1.30**	**−0.03**	−0.25	−0.10	−0.08	−2.10	−1.12	−5.82
Gombe	**−0.23**	**0.54**	**−0.56**	**0.74**	**0.70**	**−0.05**	**−2.47**	0.65	**−0.18**	**−9.36**	**−5.47**	**−19.37**
Goure	**−0.25**	**0.56**	**−0.62**	**0.68**	**1.26**	**−0.04**	−0.81	0.07	−0.13	−1.52	−0.68	−4.48
Jos	**−0.24**	**0.30**	**−0.37**	**0.61**	0.26	**−0.04**	**−4.80**	0.77	**−1.19**	**−19.40**	**−5.90**	−39.02
Kaduna	**−0.20**	**0.25**	**−0.36**	**0.49**	0.19	**−0.04**	**−3.11**	0.61	**−0.23**	**−9.83**	**−5.14**	−27.67
Kano	**−0.24**	**0.36**	**−0.37**	**0.53**	**0.46**	−0.02	−2.01	0.10	**−0.16**	**−8.83**	0.13	−22.91
Katsina	**−0.31**	**0.57**	**−0.55**	**0.60**	**1.21**	**−0.02**	−1.77	0.66	**−0.09**	−0.80	−1.38	−9.34
Magaria	**−0.29**	**0.58**	**−0.57**	**0.62**	**1.35**	−0.02	−2.34	−0.25	**−0.25**	−4.19	−2.33	−13.91
Maiduguri	**−0.16**	**0.40**	**−0.50**	**0.68**	**0.48**	**−0.03**	**−2.96**	0.71	−0.09	**−4.79**	−1.54	−11.62

(*continued on next page*)

Table A.2 (*continued*)

a. Near future analysis at RCP4.5 (2020–2050)

Stations	Temperature Indices						Rainfall Indices					
	tx10p	tx90p	tn10p	tn90p	wsdi	dtr	rx5day	cdd	cwd	r95p	r99p	prcptot
Maine-Soroa	**−0.25**	**0.57**	**−0.58**	**0.61**	**1.37**	**−0.02**	−0.18	0.61	0.00	−1.58	−0.91	−4.60
Nguru	**−0.21**	**0.36**	**−0.56**	**0.56**	**0.52**	**−0.02**	−1.10	0.85	−0.02	−2.07	−0.39	**−6.06**
Potiskum	**−0.27**	**0.61**	**−0.59**	**0.64**	**1.31**	**−0.02**	−0.54	0.62	**−0.31**	−1.28	0.62	**−8.63**
Zinder	**−0.28**	**0.58**	**−0.59**	**0.62**	**1.37**	−0.02	−0.94	−0.78	−0.15	−1.99	−0.60	−5.17

b. Far future analysis at RCP4.5 (2060–2090)

Stations	Temperature Indices						Rainfall Indices					
	tx10p	tx90p	tn10p	tn90p	wsdi	dtr	rx5day	cdd	cwd	r95p	r99p	prcptot
Bauchi	**−0.33**	0.23	**−0.49**	**0.45**	0.49	0.00	**2.62**	−0.04	0.15	**9.85**	2.01	**23.56**
Diffa	**−0.29**	**0.28**	**−0.41**	**0.39**	0.34	−0.01	0.95	1.30	**−0.11**	0.90	1.02	0.98
Gombe	**−0.44**	**0.37**	**−0.47**	**0.41**	0.26	0.00	2.28	0.00	**0.11**	**7.98**	0.85	**13.32**
Goure	**−0.34**	**0.28**	**−0.47**	**0.37**	0.45	**−0.03**	−0.89	**1.91**	−0.06	−1.58	−0.35	−1.67
Jos	**−0.50**	**0.39**	**−0.37**	**0.42**	**0.33**	**−0.03**	**3.28**	0.01	**0.57**	**11.72**	**4.96**	**23.33**
Kaduna	**−0.45**	**0.38**	**−0.43**	**0.46**	**0.39**	−0.01	1.25	0.05	0.11	4.65	2.65	**10.05**
Kano	**−0.50**	**0.43**	**−0.38**	**0.35**	0.24	**−0.04**	−1.10	−0.12	0.04	−1.93	−0.17	3.99
Katsina	**−0.35**	**0.27**	**−0.41**	**0.38**	0.47	**−0.03**	−0.62	0.84	−0.03	−2.44	−0.72	−0.56
Magaria	**−0.37**	**0.31**	**−0.42**	**0.35**	0.46	**−0.02**	−0.08	**1.98**	−0.09	0.30	−0.18	1.23
Maiduguri	**−0.31**	**0.30**	**−0.44**	**0.36**	0.19	**−0.05**	1.64	0.50	0.00	3.45	1.62	4.33
Maine-Soroa	**−0.33**	**0.28**	**−0.46**	**0.43**	0.46	**−0.03**	−0.13	0.15	−0.02	1.31	−0.33	0.63
Nguru	**−0.31**	**0.27**	**−0.42**	**0.40**	**0.35**	**−0.05**	0.76	**1.89**	−0.02	−0.89	0.04	1.93
Potiskum	**−0.35**	**0.28**	**−0.43**	**0.33**	0.45	0.00	0.53	0.95	**0.16**	2.52	1.64	3.51
Zinder	**−0.33**	**0.29**	**−0.45**	**0.42**	0.33	0.00	**−3.61**	**2.27**	−0.01	**−6.76**	**−5.07**	−6.24

c. Near future analysis at RCP8.5 (2020–2050)

Stations	Temperature Indices						Rainfall Indices					
	tx10p	tx90p	tn10p	tn90p	wsdi	dtr	rx5day	cdd	cwd	r95p	r99p	prcptot
Bauchi	**−0.64**	**0.77**	**−0.91**	**1.12**	**1.04**	**−0.03**	−1.60	0.31	**−0.40**	**−8.69**	−0.67	**−28.17**
Diffa	**−0.53**	**0.77**	**−0.87**	**0.98**	**1.51**	**−0.03**	−1.94	−0.97	−0.08	−6.67	**−3.02**	**−11.46**
Gombe	**−0.45**	**0.80**	**−0.79**	**1.24**	**1.01**	**−0.04**	−2.71	0.39	**−0.22**	−6.74	−3.30	**−22.67**
Goure	**−0.55**	**0.76**	**−0.87**	**0.98**	**1.36**	**−0.05**	−1.54	−1.22	−0.20	**−5.57**	−0.79	**−9.64**
Jos	**−0.53**	**0.47**	**−0.68**	**0.93**	**0.39**	**−0.06**	**−2.78**	0.50	−0.34	**−9.75**	**−5.27**	**−36.46**
Kaduna	**−0.46**	**0.45**	**−0.62**	**0.99**	**0.45**	**−0.06**	−0.97	0.63	−0.21	**−7.19**	−3.24	**−24.92**
Kano	**−0.56**	**0.66**	**−0.53**	**0.86**	**1.16**	**−0.03**	−1.93	0.66	−0.03	−5.32	**−5.78**	**−27.37**
Katsina	**−0.57**	**0.81**	**−0.80**	**0.96**	**1.51**	**−0.03**	**−2.34**	−0.17	−0.08	**−5.69**	−2.04	**−14.66**
Magaria	**−0.56**	**0.81**	**−0.81**	**0.93**	**1.59**	**−0.02**	−1.93	−1.13	**−0.34**	**−8.00**	−2.13	**−19.72**
Maiduguri	**−0.45**	**0.56**	**−0.86**	**1.00**	**0.74**	**−0.05**	−1.87	0.20	−0.03	**−7.18**	**−3.08**	**−15.67**
Maine-Soroa	**−0.57**	**0.75**	**−0.85**	**0.96**	**1.32**	**−0.03**	−1.00	0.92	−0.04	−1.58	−1.39	**−9.58**
Nguru	**−0.46**	**0.59**	**−0.84**	**0.93**	**0.89**	**−0.04**	−1.43	0.89	−0.07	−4.10	−1.95	**−12.65**
Potiskum	**−0.60**	**0.81**	**−0.86**	**1.01**	**1.34**	**−0.02**	**−3.44**	0.49	**−0.29**	**−8.56**	**−6.26**	**−18.87**
Zinder	**−0.53**	**0.79**	**−0.82**	**0.93**	**1.32**	−0.02	−2.65	−1.17	0.00	**−9.16**	−2.65	**−17.10**

d. Far future analysis at RCP8.5 (2060–2090)

Stations	Temperature Indices						Rainfall Indices					
	tx10p	tx90p	tn10p	tn90p	wsdi	dtr	rx5day	cdd	cwd	r95p	r99p	prcptot
Bauchi	**−0.81**	**0.87**	**−1.36**	**1.28**	**1.44**	0.00	**3.89**	0.61	**0.15**	**14.05**	**5.18**	**34.01**
Diffa	**−0.70**	**0.81**	**−1.16**	**1.15**	**1.58**	−0.01	1.23	1.85	0.11	4.99	1.69	**12.64**
Gombe	**−0.92**	**1.10**	**−1.31**	**1.34**	**1.62**	**−0.02**	**5.40**	0.61	**0.23**	**17.95**	**7.28**	**36.04**
Goure	**−0.70**	**0.79**	**−1.14**	**1.18**	**1.65**	**−0.02**	1.07	**1.93**	−0.06	**3.52**	1.67	**9.38**
Jos	**−0.75**	**1.12**	**−1.19**	**1.30**	**1.35**	**−0.02**	**4.27**	0.54	**0.87**	**20.76**	**7.56**	**48.35**
Kaduna	**−0.69**	**1.07**	**−1.12**	**1.34**	**1.13**	**−0.03**	**2.56**	0.65	0.14	11.07	3.93	**28.84**
Kano	**−0.80**	**1.05**	**−1.18**	**1.10**	**1.42**	**−0.03**	1.64	0.50	0.00	3.45	1.62	4.33
Katsina	**−0.77**	**0.80**	**−1.26**	**1.20**	**1.53**	**−0.03**	2.52	0.94	**0.23**	**5.41**	**2.69**	**18.06**
Magaria	**−0.87**	**0.83**	**−1.25**	**1.16**	**1.76**	**−0.02**	**4.07**	**2.22**	**0.32**	**12.71**	5.79	**27.18**
Maiduguri	**−0.66**	**0.88**	**−1.24**	**1.17**	**1.19**	**−0.05**	**3.46**	0.11	**0.14**	**8.82**	**2.92**	**17.43**
Maine-Soroa	**−0.71**	**0.79**	**−1.18**	**1.13**	**1.63**	**−0.03**	**2.07**	0.50	0.04	**5.44**	**2.09**	**13.87**
Nguru	**−0.63**	**0.72**	**−1.20**	**1.12**	**1.21**	**−0.04**	1.75	0.53	0.05	**6.97**	**4.16**	**14.99**
Potiskum	**−0.77**	**0.76**	**−1.27**	**1.16**	**1.53**	**0.02**	**4.06**	0.59	0.14	**14.69**	**4.96**	**26.08**
Zinder	**−0.69**	**0.78**	**−1.19**	**1.13**	**1.59**	**0.02**	2.92	**3.10**	**0.33**	**8.96**	4.65	**21.24**

References

Abatan, A., Abiodun, B., Gutowski, W., Rasaq-Balogun, S., 2017a. Trends and variability in absolute indices of temperature extremes over Nigeria: linkage with NAO. Int. J. Climatol. 38 (2), 593–612.

Abatan, A., Osayomi, T., Akande, S., Abiodun, B., Gutowski, W., 2017b. Trends in mean and extreme temperatures over Ibadan, Southwest Nigeria. Theor. Appl. Climatol. 131 (3–4), 1261–1272.

Abiodun, B., Adegoke, J., Abatan, A., Ibe, C., Egbebiyi, T., Engelbrecht, F., Pinto, I., 2017. Potential impacts of climate change on extreme precipitation over four African coastal cities. Climatic Change 143 (3–4), 399–413.

Acquaotta, F., Fratianni, S., 2014. The importance of the quality and reliability of the historical time series for the study of climate change. Rev. Bras. Climatol. 10, 20–38.

Acquaotta, F., Fratianni, S., Venema, V., 2016. Assessment of parallel precipitation measurements networks in Piedmont, Italy. Int. J. Climatol. https://doi.org/10.1002/joc.4606.

Adeyeri, O., Lawin, A., Laux, P., Borne, M., 2018. Boxplot of climate indices consisting of 8 climate models with the ensemble mean for different climatic station in the Komadugou-Yobe basin, Lake Chad region, West Africa. Mendeley Data v2. https://doi.org/10.17632/97p2x3hjst.2.

Adeyeri, O., Ishola, K., Okogbue, E., 2017a. Climate change and coastal floods: the susceptibility of coastal areas of Nigeria. J. Coast. Zone Manag. 20, 443.

Adeyeri, O., Lamptey, B., Lawin, A., Sanda, I., 2017b. Spatio-Temporal precipitation trend and homogeneity analysis in Komadugu-Yobe basin, lake Chad region. J. Climatol. Weath. Forecast. 5, 214.

Adeyeri, O., Okogbue, E., Akinluyi, F., 2016. Mapping evapotranspiration for different landcover in the Lake Chad region of Nigeria using landsat datasets. J. Rems. Tech. 4 (1), 58–69.

Aguilar, E., Auer, I., Brunet, M., Peterson, T., Wieringe, J., 2003. Guidelines on Climate Metadata and Homogenization. WMO/TD No. 1186. .

Akinsanola, A., Ajayi, V., Adejare, A., Adeyeri, O., Gbode, I., Ogunjobi, K., Nikulin, G., Abolude, A., 2017. Evaluation of rainfall simulations over West Africa in dynamically downscaled CMIP5 global circulation models. Theor. Appl. Climatol. https://doi.org/10.1007/s00704-017-2087-8.

Alamou, E., Obada, E., Afouda, A., 2017. Assessment of future water resources availability under climate change scenarios in the mékrou basin, Benin. Hydrology 4 (4), 51.

Alexandersson, H., Moberg, A., 1997. Homogenization of Swedish temperature data. Homogeneity test for linear trends. Int. J. Climatol. 17, 25–34.

Attogouinon, A., Lawin, A., M'Po, Y., Houngue, R., 2017. Extreme precipitation indices trend assessment over the upper oueme river valley-(Benin). Hydrology 4 (4), 36.

Barbara, C., Victor, V., Annemarie, L., Konrad, A., Ingeborg, A., Johanna, N., 2018. Intercomparison of methods to homogenize daily relative humidity. Int. J. Climatol. https://doi.org/10.1002/joc.5488.

Dieng, D., Smiatek, G., Bliefernicht, J., Heinzeller, D., Sarr, A., Gaye, A.T., Kunstmann, H., 2017. Evaluation of the COSMO-CLM high-resolution climate simulations over West Africa. Geophys. Res. 122, 1437–1455.

Domonkos, P., Coll, J., 2018. Impact of missing data on the efficiency of homogenisation: experiments with ACMANTv3. Theor. Appl. Climatol. https://doi.org/10.1007/s00704018-2488-3.

Domonkos, P., 2014. The ACMANT2 software package. Eighth seminar for homogenization and quality control in climatological databases. WMO-WCDMP 84, 46–72.

Domonkos, P., Coll, J., 2017. Homogenisation of temperature and precipitation time series with ACMANT3: method description and efficiency tests. Int. J. Climatol. 37, 1910–1921.

Domonkos, P., Efthymiadi, D., 2013. Development and testing of homogenisation methods: moving parameter experiments with ACMANT. Adv. Sci. Res. 10, 43–50.

Domonkos, P., 2015. Homogenization of precipitation time series with ACMANT. Theor. Appl. Climatol. 122, 303–314.

Domonkos, P., Venema, V., Mestre, O., 2011. Efficiencies of homogenisation methods: our present knowledge and its limitation. In: Seventh Seminar for Homogenisation and Quality Control in Climatological Databases, WMO-WCDMP, vol. 78. pp. 19–32.

Dosio, A., Panitz, H., 2016. Climate change projections for CORDEX-Africa with COSMO-CLM regional climate model and differences with the driving global climate models. Clim. Dynam. 46 (5–6), 1599–1625.

Engelbrecht, F., McGregor, J., Engelbrecht, C., 2009. Dynamics of the conformal-cubic atmospheric model projected climate-change signal over southern africa. Int. J. Climatol. 29 (7), 1013–1033.

Gbode, I., Adeyeri, O., Menang, K., Insitful, J., Ajayi, V., Omotosho, J., Akinsanola, A., 2018. Observed changes in climate extremes in Nigeria. Meteorol. Appl submitted for publication.

Gubler, S., Hunziker, S., Begert, M., Croci-Maspoli, M., Konzelmann, K., Brönnimann, B., Schwierz, C., Oria, C., Rosas, G., 2017. The influence of station density on climate data homogenization. Int. J. Climatol. 37, 4670–4683.

Gudmundsson, L., Bremnes, J., Haugen, J., Engen-Skaugen, T., 2012. Technical Note: downscaling RCM precipitation to the station scale using statistical transformations: a comparison of methods. Hydrol. Earth Syst. Sci. 16 (9), 3383–3390.

Im, E., Jung, I., Bae, D., 2011. The temporal and spatial structures of recent and future trends in extreme indices over Korea from a regional climate projection. Int. J. Climatol. 31, 72–86.

IUCN, 2006. Lake Chad basin commission. In: The Statesman's Yearbook 2007 (Hg. B. Turner). Palgrave Macmillan UK, London, pp. 64.

Klutse, B., Sylla, M., Diallo, I., Sarr, A., Dosio, A., Diedhiou, A., Kamga, A., Lamptey, B., Ali, A., Gbobaniyi, E., Owusu, K., Lennard, C., Hewitson, B., Nikulin, G., Panitz, H., Büchner, M., 2014. Daily characteristics of West African summer monsoon precipitation in CORDEX simulations. Theor. Appl. Climatol. https://doi.org/10.1007/s00704-014-1352-3.

Lebel, T., Ali, A., 2009. Recent trends in the central and western Sahel rainfall regime (1990-2007). J. Hydrol. 375 (1–2), 52–64.

Lindau, R., Venema, V., 2013. On the multiple breakpoint problem and the number of significant breaks in homogenization of climate records. Idojaras Q. J. Hung. Meteorol. Serv. 117, 1–34.

Lindau, R., Venema, V., 2016. The uncertainty of break positions detected by homogenization algorithms in climate records. Int. J. Climatol. 36, 576–589.

Ly, M., Traore, S., Alhassane, A., Sarr, B., 2013. Evolution of some observed climate extremes in the West African Sahel. Weather Clim. Extreme 1, 19–25.

Lyon, B., DeWitt, D., 2012. A recent and abrupt decline in the East African long rains. Geophys. Res. Lett. 39 (2), L02702.

Mason, S., Joubert, A., 1997. Simulated changes in extreme rainfall over southern africa. Int. J. Climatol. 17 (3), 291–301.

Nikulin, G., Jones, C., Giorgi, F., Asrar, G., Büchner, M., Cerezo-Mota, R., Christensen, O.B., Déqué, M., Fernandez, J., Hänsler, A., van Meijgaard, E., Samuelsson, P., Sylla, M., Sushama, L., 2012. Precipitation climatology in an ensemble of CORDEX-africa regional climate simulations. J. Clim. 25 (18), 6057–6078.

Odunuga, S., Okeke, I., Omojola, A., Oyebande, L., 2011. Hydro-climatology: Variability and Change. IAHS Publ, pp. 344.

Pérez-Zanón, N., Sigró, J., Domonkos, Ashcroft, L., 2015. Comparison of HOMER and ACMANT homogenization methods using a central Pyrenees temperature dataset. Adv. Sci. Res. 12, 111–119.

Peterson, T., Easterling, D., Karl, T., Groisman, P., Nicholls, N., Plummer, N., Torok, S., Auer, I., Boehm, R., Gullett, D., Vincent, L., Heino, R., Tuomenvirta, H., Mestre, O., Szentimrey, T., Salinger, J., Forland, E., Hassen-Bauer, I., Alexandersson, H., Jones, P., Parker, D., 1998. Homogeneity adjustments of in situ atmospheric climate data: a review. Int. J. Climatol. 18, 1493–1517.

Pinto, I., Lennard, C., Tadross, M., Hewitson, B., Dosio, A., Nikulin, G., Panitz, H., Shongwe, M., 2016. Evaluation and projections of extreme precipitation over southern Africa from two CORDEX models. Climatic Change 135 (3–4), 655–668.

Poli, P., Hersbach, H., Dee, D.P., Berrisford, P., Simmons, A.J., Vitart, F., Laloyaux, P., Tan, D.G., Peubey, C., Thépaut, J., Trémolet, Y., Hólm, E.V., Bonavita, M., Isaksen, L., Fisher, M., 2016. ERA-20C: an atmospheric reanalysis of the twentieth century. J. Clim. 29, 4083–4097.

Samuelsson, P., Jones, C., Willén, U., Ullerstig, A., Gollvik, S., Hansson, U., et al., 2011. The Rossby Centre regional climate model RCA3: model description and performance. Tellus A 63, 4–23.

Sarr, B., 2011. Return of heavy downpours and floods in a context of changing climate. In: AGRHYMET Monthly Bulletin, Special Issue, pp. 9–11.

Shepard, D., 1968. A two-dimensional interpolation function for irregularly-spaced data. In: Blue, R.B., Rosenberg, A.M. (Eds.), The 1968 23rd ACM National Conference, pp. 517–524.

Shongwe, M., van Oldenborgh, G., van den Hurk, B., Boer, B., Coelho, C., van Aalst, M., 2010. Projected changes in mean and extreme precipitation in Africa under global warming. Part 1: southern Africa. J. Clim. 22 (13), 3819–3837.

Teutschbein, C., Seibert, J., 2013. Is bias correction of regional climate model (RCM) simulations possible for non-stationary conditions? Hydrol. Earth Syst. Sci. 17 (12), 5061–5077.

Thompson, J., Polet, G., 2000. Hydrology and land use in a sahelian floodplain wetland. Wetlands 20 (4), 639–659.

Trewin, B., 2010. Exposure, instrumentation, and observing practice effects on land temperature measurements. Wiley Interdiscip. Rev.: Climatic Change 4, 490–506.

Venema, V., Mestre, O., Aguilar, E., Auer, I., Guijarro, J., Domonkos, P., Vertacnik, G., Szentimrey, T., Štepánek, P., Zahradnicek, P., Viarre, J., Müller-Westermeier, G., Lakatos, M., Williams, C., Menne, M., Lindau, R., Rasol, D., Rustemeier, E., Kolokythas, K., Marinova, T., Andresen, L., Acquaotta, F., Fratianni, S., Cheval, S., Klancar, M., Brunetti, M., Gruber, C., Duran, M., Likso, T., Esteban, P., Brandsma, T., 2012. Benchmarking monthly homogenization algorithms. Clim. Past 8, 89–115.

Vincent, L., Peterson, T., Barros, V., Marino, M., Rusticucci, M., Carrasco, G., Ramirez, E., Alves, L., Ambrizzi, T., Berlato, M., Grimm, A., Marengo, J., Molion, L., Moncunill, D., Rebello, E., Anunciação, Y., Quintana, J., Santos, J., Baez, J., Coronel, G., Garcia, J., Trebejo, I., Bidegain, M., Haylock, M., Karoly, D., 2005. Observed trends in indices of daily temperature extremes in south America 1960-2000. J. Clim. 18 (23), 5011–5023.

Xu, Chong-Hai, Xu, Y., 2012. The projection of temperature and precipitation over China under RCP scenarios using a CMIP5 multi-model ensemble. Atmos. Oceanic Sci. Lett. 5, 527–533.

Yira, Y., Diekkrüger, B., Steup, G., Bossa, A.Y., 2017. Impact of climate change on hydrological conditions in a tropical West African catchment using an ensemble of climate simulations. Hydrol. Earth Syst. Sci. 21, 2143–2161.

Zhang, Y., Xu, Y., Dong, W., Cao, L., Sparrow, M., 2006. A future climate scenario of regional changes in extreme climate events over China using the PRECIS climate model. Geophys. Res. Lett. 33, L24702.

Zhang, X., Yang, F., 2004. RClimDex (1.0) User Manual, Climate Research Branch Environment, Ontario, Canada. http://etccdi.pacificclimate.org/software.shtml, Accessed date: 13 March 2017.